EXTENDING THE ROLE OF CAPNOGRAPHY DURING MECHANICAL VENTILATION

PhD Thesis

Anita Korsós, MD

Doctoral School of Multidisciplinary Medical Sciences
University of Szeged

Supervisors:

Barna Babik, MD, PhD
Department of Anaesthesiology and Intensive Therapy, University of Szeged

Ferenc Peták, PhD, DSc
Department of Medical Physics and Informatics, University of Szeged

2022

List of scientific papers included in this thesis

Study I.

Korsós A, Peták F, Südy R, Schranc Á, Fodor GH, Babik B. Use of capnography to verify emergency ventilator sharing in the COVID-19 era. *Respir Physiol Neurobiol*. 2021; 285: 103611. doi: 10.1016/j.resp.2020.103611. [IF: 2.821]

Study II.

Südy R, Peták F, Kiss L, Balogh ÁL, Fodor GH, **Korsós A**, Schranc Á, Babik B. Obesity and diabetes: similar respiratory mechanical but different gas exchange defects. *Am J Physiol Lung Cell Mol Physiol.* 2021; 320: L368-L376. doi: 10.1152/ajplung.00439.2020. [IF:6.011]

List of scientific papers related to the thesis

Korsós A, Kupcsulik Sz, Lovas A, Hankovszky P, Molnár T, Szabó Zs, Babik B. Diagnostic consideration and bedside estimation of the prognosis in COVID-19 patients. *Orv. Hetil.* 2020; 161: 667- 671. doi: 10.1556/650.2020.31815. [IF: 0.540]

Wendel Garcia PD, Aguirre-Bermeo H, Buehler PK, Alfaro-Farias M, Yuen B, David S, Tschoellitsch T, Wengenmayer T, **Korsós A**, Fogagnolo A, *et al.* (RISC-19-ICU Investigators): Implications of early respiratory support strategies on disease progression in critical COVID-19: a matched subanalysis of the prospective RISC-19-ICU cohort. *Crit Care* 2021; 25, 1752. doi: 10.1186/s13054-021-03580-y [IF:19.346]

Kovács BN, Südy R, Peták F, Balogh ÁL, Fodor HG, Tolnai J, **Korsós A**, Schranc Á, Lengyel C, Babik B. Respiratory consequences of obesity and diabetes. *Orv. Hetil.* 2022; 163: 63-73. doi: 10.1556/650.2022.32335. [IF: 0.707]

Lovas A, Hankovszky P, **Korsós A**, Kupcsulik S, Molnár T, Szabó Z, Babik B. Importance of the imaging techniques in the management of COVID-19-infected patients. *Orv. Hetil.* 2020; 161: 672-677. doi: 10.1556/650.2020.31814. [IF: 0.540]

TABLE OF CONTENTS

BACKGROUND 8
Multimodal patient monitoring in perspective 8
Capnography 9
Definition 9
History of capnography 9
Measurement principle 10
Types of capnography 10
Mainstream vs. sidestream techniques 10
Time vs. volumetric capnography 11
The capnogram curve: phases and shape factors 11
Anatomic dead space according to Fowler 14
Physiologic dead space according to Bohr 14
Physiologic dead space according to Enghoff 14
Other parameters assessed by capnography 15
Alveolo-arterial pCO_2 difference ($PaCO_2$-$PetCO_2$) 15
Capnogram angles 15
Minute expiration of CO_2 16
Clinical indications of capnography and capnometry 16
Securing the airway and patient safety 16
Monitoring of clinical parameters 16
Capnography beyond tube position and patient safety 17
The SARS-CoV2 pandemic 18
Respiratory consequences of obesity and diabetes 19
AIMS AND HYPOTHESES 21
Study I.: 21
To establish the use of capnography to verify emergency ventilator sharing in the COVID-19 era by 21
MATERIALS AND METHODS 22
Study I.: Use of capnography to verify emergency ventilator sharing in the COVID-19 era 22
The experimental setup 22
Data acquisition 24
Simulation study 24
Measurement protocol 25

Study II.: Obesity and diabetes: similar respiratory mechanical, but different gas exchange abnormalities 26
Ethical considerations 26
Patients and study groups 27
Anaesthesia and patient monitoring 27
Recording and analyses of the volumetric capnogram 27
Measurement protocol 28
Statistical analyses 28
Study I.: Use of capnography to verify emergency ventilator sharing in the COVID-19 era 30
Study II.: obesity and diabetes: similar respiratory mechanical, but different gas exchange abnormalities 35
DISCUSSION 38
Study I.: Use of capnography to verify emergency ventilator sharing in the COVID-19 era 39
Study II. Obesity and diabetes: similar respiratory mechanical but different gas exchange defects 41
Effects of diabetes on respiratory function 41
Effects of obesity on respiratory function 42
SUMMARY AND CONCLUSIONS 43
AKNOWLEDGEMENT 45

LIST OF FIGURES AND TABLES

Figure 1. Representative time and volumetric capnograms. 12
Figure 2. Volumetric capnogram with the graphical representation of the derived parameters. 15
Figure 3. Scheme of the experimental setup for ventilation sharing. 23
Figure 4. Patient flow chart for Study II. 26
Table 1. Mechanical parameters obtained during ventilator sharing. 30
Figure 5. Representative volume, capnogram (PCO_2), airflow and pressure curves. 31
Figure 6. Ventilation parameters obtained in ventilator sharing. 33
Figure 7. Results obtained from the simulation study. 34
Table 2. Patient characteristics. 35
Figure 8. Respiratory mechanical data in patients with diabetes and/or obesity. 36
Figure 9. Capnography data in patients with diabetes and/or obesity. 37
Figure 10. Gas exchange data in patients with diabetes and/or obesity. 38

LIST OF ABBREVIATIONS

AGEs:	advanced glycation end products
ANOVA:	analysis of variances
BL:	baseline
BMI:	body-mass index
C:	compliance of the respiratory system
C_{LC}:	compliance on low-compliance side
C_{HR}:	compliance on high-resistance side
COPD:	chronic obstructive pulmonary disease
COVID-19:	coronavirus disease 2019
ECG:	electrocardiography
ET:	endotracheal
ET-1:	endothelin
f:	frequency
HbA1c:	haemoglobin A1c
HR:	high resistance
LC:	low compliance
NO:	nitric oxide
PC:	pressure-controlled ventilation
PCO_2:	partial pressure of CO2
P_aCO_2:	arterial partial pressure of CO_2
PaO_2/FiO_2:	oxygenation index
P_ACO_2:	mean alveolar partial pressure of CO_2
$P_{a\text{-}et}CO_2$:	arterial to end-tidal CO_2 partial pressure gradient
$P_{\bar{E}}CO_2$:	mixed expired partial pressure of CO_2
PEEP:	positive end-expiratory pressure
$PetCO_2$:	end-tidal partial pressure of CO_2
PEF:	peak expiratory flow
PIF:	peak inspiratory flow
Ppi:	peak inspiratory pressure
Qs/Qt:	intrapulmonary shunt
R:	total respiratory system resistance

R_{LC}: resistance on low-compliance side

R_{HR}: resistance on high-resistance side

SARS-CoV2: severe acute respiratory syndrome caused by the novel coronavirus

S2: capnogram phase 2 slope

S2T: phase 2 slope in time capnogram

S2V: phase 2 slope in volumetric capnogram

S3: capnogram phase 3 slope

S3T: phase 3 slope in time capnogram

S3V: phase 3 slope in volumetric capnogram

τ: time constant

Tcap: time capnography

T2DM: type 2 diabetes mellitus

V': airflow

V/Q: ventilation/perfusion ratio

VC: volume-controlled ventilation

V_D: ventilation dead space

V_{DE}: Enghoff's dead space

V_{DF}: Fowler's dead space

V_{DB}: Bohr's dead space

V_T: tidal volume

Vcap: volumetric capnography

$V'CO_2$: amount of exhaled CO_2 in 1 min

X: reactance

Z: impedance

Z_{LC}: impedance on low-compliance side

Z_{HR}: impedance on high-resistance side

BACKGROUND

Multimodal patient monitoring in perspective

The optimal management of patients requiring general anaesthesia and/or intensive therapy poses a major challenge for health care providers. Such patients frequently suffer from complex pathologies necessitating close monitoring of organ function to decrease morbidity and to avoid mortality. The occurrence of these morbidities often leads to multiorgan failure, which severely impairs patient outcome. The early recognition of pathological processes is crucial and allows for immediate intervention. Therefore, the multimodal monitoring of organ functions is of paramount importance in facilitating the best clinical decision, thereby optimizing patient care. Such multimodal monitoring enables clinicians to gain immediate, complex, and specific information regarding the current status of the patient in the most possible aspects. It is noteworthy, however, that some of the monitoring modalities themselves may require invasive intervention, and/or may involve time consuming instrumentation, and may not be specific or sensitive enough to accurately interpret the derived data.

Recent advancements in medical technology allowed for the introduction of complex monitoring modalities, such a bedside medical imaging technique. Moreover, simple and safe and devices have become widely available for clinician uses in daily practice. Such instruments are geared towards avoiding invasivity while utilising modern information technology. This general trend applies for patient monitoring in anaesthesia and the critical care setting, where multimodal non-invasive monitoring is of particular importance attaining fast and precise information necessary for diagnostic, therapeutic and prognostic purposes. Therefore, advanced patient monitoring improves perioperative outcomes, and this is reflected in the national and international guidelines recommending the perioperative use of multimodal monitoring systems.

Noninvasive monitoring of gas exchange and ventilation is an essential component of general anaesthesia and intensive therapy. Technologies that support the noninvasive monitoring of expired CO_2 and inspired O_2 have existed for decades. Monitoring of the numeric value of end-tidal CO_2 ($PetCO_2$) expressed as either a partial pressure (mmHg, kPa) or as a percentage fraction of the expired gas is referred to as capnometry. Conversely, capnography refers to the continuous, breath-by-breath display of expired CO_2 concentration plotted against time or expired gas volume.

The monitoring airway patency and the adequacy of ventilation in ventilated patients are the most common and acknowledged indications for capnography and capnometry, and these contribute greatly to patient safety. However, technological refinement of capnography enables its application to a broader indication, which subsequently fosters methodological developments in ventilation therapy and a better understanding of complex respiratory disorders.

Capnography

Definition

Capnography is a non-invasive, continuous, online, dynamic, bedside, effort- and cooperation independent, simple to use, inexpensive, numeric and graphical analysis of the exhaled CO_2 concentration. Registration of expired CO_2 breath-by-breath over time or in the volume domain can be considered as an indicator curve of lung ventilation. Accordingly, this monitoring modality detects technical complications in the ventilator circuit, and can is able to reveal defects in alveolar ventilation and/or in matching ventilation to perfusion (1, 2).

History of capnography

The measurement of exhaled CO_2 concentration with infrared spectrophotometry has been available since the 1940s (3). The first bedside application of infrared CO_2-meters was developed in the 1950s (4). In the 1960s, the use of capnography as a monitoring tool gained some interest in Europe (5). However, a survey at the World Congress on Intensive Care Medicine in the U. S. in 1978 revealed that two out of five anaesthesiologists there no be no promising future for capnography (6). The change in approach dates to the 1980s, when capnography became widely available as a monitoring modality worldwide (7).

After the general worldwide recognition of the clinical diagnostic value of capnography, this technique became one of the prevailing bedside patient monitoring modalities, in addition to the other well-established techniques, such as ECG and pulse oximetry. Since then, capnography has unquestionable value in a wide array of medical disciplines, including anaesthesiology and intensive care (8, 9), pulmonology (10, 11), emergency medicine (12, 13), paediatrics (14), and sleep medicine (9, 13). Moreover, capnography is an essential part of the life-support monitoring modality during resuscitation and patient transport. It is also worth noting, however, that despite the widespread use of capnography, the scope of its use in clinical

practice remained fairly narrow and is limited mainly to verifying tube position and/or to assessing respiratory minute volume.

Recently, research performed by our group (8, 15-18) and other laboratories (19-21) has demonstrated the extended potential of capnography since exhaled CO_2 can be considered an endogenous indicator gas. This bedside approach provides additional essential information regarding the physiology and pathophysiology of lung ventilation and ventilation/perfusion matching, which is of major importance during mechanical ventilation (8, 15-21).

Measurement principle

Quantitative methods to assess the CO_2 content of a gas mixture are applied in infrared spectroscopy based on the Raman or Beer-Lambert laws (22). Briefly, the exhaled CO_2 absorbs infrared light of 4.3 μm wavelength in a great quantity, with only minimal interference with other gases (1). Therefore, the magnitude of the absorbed infrared light is proportional to the partial pressure of CO_2 (pCO_2) in the given gas mixture.

Types of capnography

Capnography techniques can be distinguished based on the relationships between the gas sampling site and the analyser.

Mainstream vs. sidestream techniques

Mainstream capnography measures the pCO_2 in a "near-patient" position, since the cuvette is located between the endotracheal tube and Y-piece of the ventilation circuit (23, 24). This technique is fast and accurate, but increases the instrumental dead space (25), may exert a pulling force on the ET-tube, and the transparent cuvette must be heated to avoid condensation of exhaled water-vapour on the measurement window (26).

As an alternative measurement technique, sidestream capnography uses a sample tube via a lightweight T-piece located by the patient's head and analyses the gas mixture in a monitor away from the patient (23, 24). This approach can also be used to measure the concentration of other gases (e.g., oxygen, volatile anaesthetic gases). Furthermore, it can be readily applied in spontaneously breathing patients. The potential disadvantage of this method is the possible moisture condensation that may obstruct the long and thin sampling tube (23), and the presence of a delay in the pCO_2 signal, which subsequently decreases the dynamic response time of the

capnograph (16, 24, 27). There is also a risk of underestimating the $PetCO_2$ in cases of tachypnoea (28).

Time vs. volumetric capnography

Another possibility to differentiate capnography is based on the expression of the breath-by-breath CO_2 concentration against an independent variable, such as time or expired gas volume.

Time capnography (Tcap) displays the intratidal CO_2 concentration changes as a function of time. This technique is easy-to-use and straightforward to interpret in everyday clinical practice. Its use is widespread in ventilated patients, where it provides information about the lung ventilation along with other monitoring systems (e. g., pressure, flow, volume, oxygen saturation) (1, 2, 29-31). Moreover, this modality can also be easily applied in non-intubated patients. An important limitation of the Tcap is that the alveolo-arterial CO_2 difference can only be roughly estimated, especially in the presence of emphysema or ventilation inhomogeneity, and only sudden and marked changes can be detected within a patient.

Volumetric capnography (Vcap), where the intratidal changes in pCO_2 are displayed against the expired gas volume, is available in dedicated capnographs and in novel ventilators (32-37).The Vcap is usually implemented by using a mainstream CO_2 sensor in series with a patient-near flow sensor. The prompt response time of the system allows an accurate assessment of alveolo-arterial pCO_2 difference, the ventilation dead space fractions, and the amount of the exhaled CO_2 in a minute ($V'CO_2$). Compared to Tcap, phases I and II are longer and phase III is shorter in Vcap since the expiratory flow rate exponentially decreases towards end-expiration.

The capnogram curve: phases and shape factors

The expiratory phase of the time and volumetric capnogram can be divided into three phases (Figure 1) (38).

Phase I. is identified at the beginning of expiration, where the gas mixture originates from the anatomic and/or from the instrumental dead space in the case of mechanical ventilation. Since the pCO_2 level in this phase of the capnogram is equivalent to that in the atmospheric level, the exact starting point of the expiration can only be identified from the Vcap and cannot be distinguished from Tcap recordings.

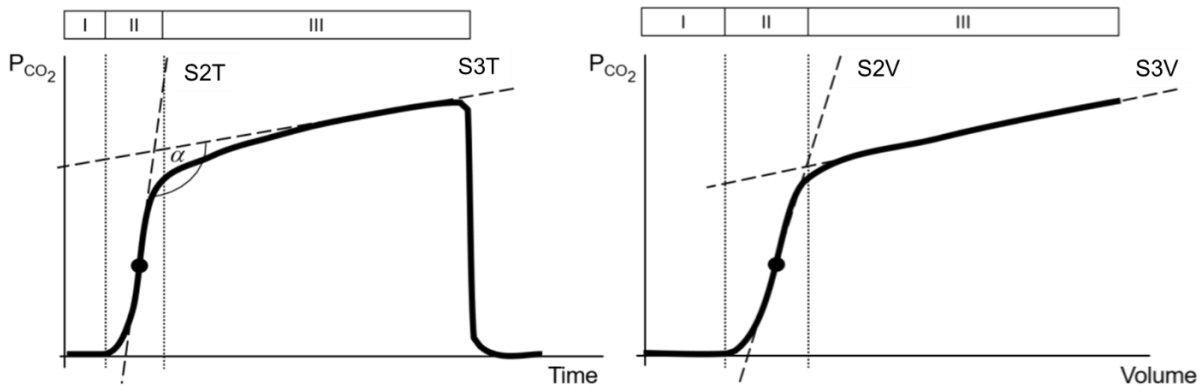

Figure 1. *Representative time and volumetric capnograms.*
Roman numerals denote capnogram phases (I-III). S2T, S2V, S3T and S3V denote phase II, and phase III slopes of time and volumetric capnograms, respectively. α determines the angle between the lines fitted to phase II and phase III.

Phase II. is the transition zone, in which the increasing concentration of CO_2 can be attributed to the diffusion and convection gas mixing between the gases originating from the dead spaces and the alveolar compartment (39). It forms the shape of an elongated upstroke, resembling a tilted letter S. The shape of phase II can be characterized by its slope in the time (S2T) or in the volumetric (S2V) capnogram. Under pathological circumstances, S2T and S2V are decreased as a consequence of diffusion- and convection-dependent heterogeneity and/or reduced lung recoil or increased airway resistance that constrains lung emptying (17). Therefore, phase 2 slope as a shape factor may indicate of abnormal lung function in emphysema, asthma bronchiale and alveolar derecruitment. (11, 40, 41).

In severe lung heterogeneity phase II is also tilted, the border between phases II and III is washed away, and the plateau almost disappears (shark-fin shape).

Phase III. refers to the CO_2 content of the gas originating from the alveolar compartment. Its shape is similar to a gradually ascending plateau with a slope in the time domain of 2-3 mmHg/s or 0.3-0.4 kPa/s (S3T), or in the volumetric domain of 0.5-2.5 kPa/ml (16, 18)). The physiologic slope of this phase originates from the gas mixing via diffusion, and the fact that breathing is cyclic, but the capillary circulation is continuous, and CO_2 diffuses constantly to a gradually decreasing alveolar volume during expiration. Therefore, alveoli with a longer time constant will have a slightly higher CO_2 content. The highest point of this phase defines the end-tidal CO_2 concentration, with a normal value of 30-43 mmHg, or 4.0-5.7 kPa (4-5.6 vol%).

Under pathologic circumstances if a ventilation/perfusion mismatch exists, the formation of lung microcompartments with different time constants and consequently different CO_2 content may be formed in the alveoli (36). The subsequent parallel and/or sequential heterogeneities in alveolar emptying may cause a pathologic increase in S3 (2, 11, 29, 42). The phase III slope depends on the magnitude of heterogeneity in the alveolar ventilation and/or the compliance of the respiratory system. High and steep S3T or S3V is characteristic of emphysema wherein the destructed alveoli prevent each other's emptying, and the compliance of the respiratory system is low (8). In the presence of concomitant diseases e.g., heart failure or obesity, the elevated phase 3 slope may be compensated by the increased lung recoil resulting in an almost normal S3T and S3V. Accordingly, a falsely normal capnogram phase III slope may also be observed in patients with severe emphysema, if this condition is associated with low respiratory system compliance. In this case, one part of the lung may be ventilated fairly homogenously while other parts are excluded from ventilation uniformly, thereby not participating in gas exchange (8). Thus, the closing capacity is higher than the sum of the functional residual capacity and the tidal volume. This concept indicates that the phase 3 slope should be always evaluated concomitantly with the respiratory system compliance, and low S3T and S3V can be accepted as an indicator of physiological lung ventilation only in patients with normal compliance. Moreover, the phase III slope absolute values may also be falsely low in decreased pulmonary flow and/or low arterial pCO_2 ($PaCO_2$) with subsequently reduced $PetCO_2$. Such situations can occur, for example after weaning from cardiopulmonary bypass (CPB). In these cases, S3T and S3V can be normalized by dividing their values with the $PetCO_2$, thereby allowing a more precise evaluation of altered ventilation heterogeneity.

By the end of the phase III, the pCO_2 on the capnogram curve exhibits a steep drop to reach baseline, where it continues until the beginning of the next expiration. In general, dead space refers to the fraction of tidal volume that does not participate in gas exchange, as this gas compartment does not come into contact with pulmonary capillary circulation (38, 43, 44). Ventilation dead space can be expressed as an absolute gas volume, its proportion to the tidal volume (V_D/V_T) or its proportion to the minute ventilation. Dead space indices can be categorized as anatomic and physiologic parameters. Anatomic dead space refers to the extra-alveolar gas compartment residing in the conducting airways and in the ventilation circuit distant to the Y-piece. Physiologic dead space includes the anatomical dead space and the gas content of the respiratory zones that do not partake in gas exchange (43, 45, 46).

Anatomic dead space according to Fowler

The anatomic dead space according to Fowler (V_{DF}) incorporates the volume of conductive airways where gas exchange does not take place and the gas volume in the ventilator circuit behind the Y-piece (45). Its normal value is approximately 2 ml/BWkg with exact normal values depending also on the height of the patient. Tidal volume, PEEP and functional residual capacity may also influence its actual value. Its breath-by-breath measurement is based on the identification of the airway-alveolar gas front in the Vcap curve, by taking the volume expired up to the inflection point of phase II of the volumetric capnogram (*Figure 2*) (16, 47).

Physiologic dead space according to Bohr

The physiological dead space according to Bohr (V_{DB}) incorporates the anatomic dead space (V_{DF}) and the gas volume of the alveoli with decreased or no perfusion, where gas exchange is subsequently compromised or does not occur (43). Its normal value is approximately 2.2-2.5 ml/BWkg. The assessment of this dead space parameter is based on the determination of the mean expired ($P_{\bar{E}}CO_2$) and alveolar CO_2 concentrations (P_ACO_2) in the Vcap curve as follows (43, 48):

$$V_{DB}/ V_T = (P_ACO_2 - P_{\bar{E}}CO_2)/ P_ACO_2,$$

where P_ACO_2 is determined from the midpoint of phase III of the Vcap curve (49), and $P_{\bar{E}}CO_2$ is calculated as integrating the area under the Vcap curve and dividing the resulting values by the actual V_T (*Figure 2*).

Physiologic dead space according to Enghoff

The Enghoff dead space (V_{DE}) can be determined in order to estimate the ventilation/perfusion mismatch (46). Compared to Bohr's dead space, the V_{DE} also contains alveoli with maintained perfusion but decreased or no ventilation (i.e., alveolar shunt), and can be calculated as follows:

$$V_{DE}/ V_T = (P_aCO_2 - P_{\bar{E}}CO_2)/ P_aCO_2$$

where P_aCO_2 is the partial pressure of CO_2 in the arterial blood (*Figure 2*). The differences between the Enghoff and Bohr dead-space parameters ($V_{DE} - V_{DB}$) can be considered as surrogate of the intrapulmonary shunt (16, 17).

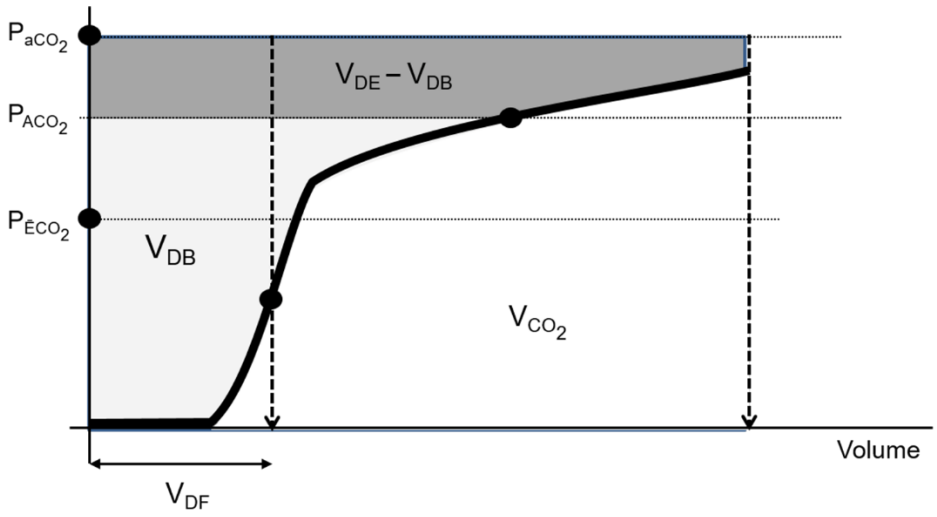

Figure 2. *Volumetric capnogram with the graphical representation of the derived parameters. VCO_2 (volume of expired CO_2 in one breath): area under curve, V_{DF} (Fowler dead space): volume expired until the inflexion point of phase II, V_{DB} (Bohr dead space): light grey area, V_{DE} (Enghoff dead space): sum of light and dark grey areas. P_aCO_2, P_ACO_2 and $P_{\bar{E}}CO_2$ refer to the arterial, mean alveolar and mean expired CO_2 partial pressures, respectively.*

Other parameters assessed by capnography

Alveolo-arterial pCO_2 difference ($PaCO_2$-$PetCO_2$)

The physiological value of $PaCO_2$-$PetCO_2$ is 2-3 mmHg. Ventilation-perfusion (V/Q) mismatch, such as shunt circulation and dead-space ventilation may increase its value. However, this difference may be reduced in the presence of a severe sequential ventilation heterogeneity. Concomitant ventilation-perfusion mismatch and sequential ventilation heterogeneity influences the $PaCO_2$-$PetCO_2$ in opposite directions and, thus, changes may neutralize each other (50). The $PaCO_2$-$PetCO_2$ may even be negative in special clinical scenarios, such as in pregnancy, extreme obesity, or after cardiopulmonary bypass, where the proportion of alveolar compartments with low ventilation/perfusion is high (51, 52).

Capnogram angles

Angle α is enclosed by phases II and III (*Figure 1*). By a standard 12.5 mm/sec monitoring speed its normal value is 100-110 degrees. The α angle may increase as a consequence of decreased S2 and/or increased S3.

Minute expiration of CO_2

The amount of expired CO_2 in one minute ($V'CO_2$) is a derived parameter from volumetric capnography by integrating the expired CO_2 concentration (39, 47, 49). Its normal value is 3 ml/Bwkg. The value may increase in sepsis, delirium and/or following exogenous administration or endogenous release of catecholamines.

Clinical indications of capnography and capnometry

Monitoring the expired CO_2 concentration is of particular importance in two major clinical areas.

Securing the airway and patient safety

Capnography can provide technical assistance in the rapid and correct positioning of the endotracheal tube or supraglottic airway devices. It may also be helpful during blind intubation and as well as the early detection of technical complication, such as the disconnection of the ventilation circuit, malpositioning of the endotracheal tube, insufficient sealing around the ET-tube cuff, or exhausted CO_2 absorbent soda (29).

Two important facts should be considered regarding the monitoring value of capnography. First, capnography is not exclusive, but rather an additional tool to facilitate correct endotracheal intubation, and should always to be supplemented with auscultation and visual inspection of chest movement (31). A second important note is that while ventilation can be monitored with capnography, it does not give direct insight into lung oxygenation (1).

Monitoring of clinical parameters

Capnography draws attention to various clinical scenarios resulting from ventilation (V) or perfusion (Q) defect or V/Q mismatch, which should be evaluated along with other clinical signs and symptoms. Capnography may provide important information during ventilator weaning by observing high or low $P_{et}CO_2$ values. Additionally, the effectiveness of muscle relaxation can be assessed from the abnormal phase III shape of the capnogram. However, in the event a jigsaw shape is seen in phase III, the distinction must be made between incomplete muscle relaxation and false suction of the sidestream capnograph during a low expiratory flow rate (53). Furthermore, capnography is an essential tool in assessing the efficacy of cardiopulmonary resuscitation (54). Monitoring of expired CO_2 concentration is also an

integral part of critical care via its ability to help in guiding ventilatory therapy even in patients without primary ventilation problems (e.g., patients with elevated intracranial pressure, fever or high carbohydrate enteral and parenteral nutrition). A sudden drop in $P_{et}CO_2$ can even raise concern for acute pulmonary embolism, however, the final diagnosis requires a complete evaluation of several supplementary clinical parameters. Trend-like changes in $P_{et}CO_2$ and/or $V'CO_2$ may indicate relative hypoventilation attributable to metabolic derangements in patients, such as in sepsis, severe systemic inflammatory response (SIRS) of various origin, and endogenous release or exogenous administration of catecholamines, or in patients with delirium. Assessment of the arterio-venous CO_2-gap can also reveal alterations in the cardiac output by factoring in the amount of exhaled CO_2.

The prominent role of capnography in patient monitoring can be attributed to the physical properties and biological aspects of CO_2. The sensing site of capnography is located more centrally than in pulse oximetry. Moreover, the diffusion capacity of the CO_2 is higher than oxygen and the changes by pulse oximetry are blunted by the sigmoid shape of the oxygen-haemoglobin dissociation curve. Therefore, sudden and profound deterioration of circulation (e.g. ventricular fibrillation, asystole) can be detected more promptly with capnography than with pulse oximetry (1, 55, 56).

Capnography beyond tube position and patient safety

Based on the methodological background detailed above, capnography provides a wide array of pathologically and clinically relevant information on both ventilation and circulation. While this monitoring technique is a standard part of multimodal monitoring modality in general anaesthesia and intensive care, the monitoring value of capnography is far from being completely utilized. Therefore, any attempt to broaden the area of clinical application of capnography contributes to improving patient safety. This simple, non-invasive and real-time monitoring modality can help steer clinical decision-making by optimizing facilities when a risk of ventilator shortage arises, such was observed during the outbreak of COVID-19 pandemic or in catastrophe medicine in combat hospitals. Furthermore, capnography allows obtaining more complete information about the cardiopulmonary status of a ventilated patient, which has particular importance in metabolic disorders with pulmonary consequences.

The SARS-CoV2 pandemic

At the beginning of 2020, the newly emerged SARS-CoV-2 virus caused a worldwide outbreak referred to as the COVID-19 pandemic. This new coronavirus may cause viral pneumonia with severe respiratory insufficiency requiring mechanical ventilation in up to 2.3-33% of the hospitalized cases. Recent epidemiologic studies about hospitalized COVID-19 patients report that the need for invasive mechanical ventilation in intensive care units ranges from 29.1% to 89.9% (57-62).

The need for ventilatory support at any critical moment is influenced by various factors. First, the virus spreads quickly in the community causing a rapid rise in the number of infected patients in a relatively short timeframe (62-64). Secondly, as critical care physicians became more familiar with the detrimental course of the COVID-19, expert opinions and consensus statements suggest initiating invasive ventilation as early as possible following respiratory symptom escalation (65-69). Finally, the majority of patients requiring mechanical ventilation generally depend on the ventilator for a prolonged period of time, which may last up to 14 days (70, 71). Under extreme circumstances, these factors may lead to a need for a high number of mechanical ventilators in order to meet the demand for the simultaneous life support.

However, the increased need for ventilators is transient, ventilatory equipment is expensive and their immediate manufacturing is proven to be difficult. Therefore, the supply is limited by economic and technical factors that may lead to a scenario when intensivists are bound to rely on the number of available ventilators in their units. Hence, the actual need for ventilators may exceed the number of available devices in case of a severe regional outbreak of COVID-19 epidemic. This may lead to an inevitable triage and a quick and difficult decision making regarding the rational utilisation of critical care means based on the promptly available information. This ultimately raises ethical concerns since the chance of survival of patients with severe respiratory insufficiency without mechanical ventilation is unquestionably lower in the presence of viral pneumonia. Therefore, it is reasonable not to dismiss the concept of ventilator splitting as a lifesaving manoeuvre, which means ventilating multiple lungs of similar patients with one apparatus. Such an emergency approach has been previously described (72-75) and more recently its feasibility was confirmed in a bench-test study (74, 75). However, many potential issues need clarification before considering this approach in clinical situations.

Respiratory consequences of obesity and diabetes

Capnography carries bedside information about the pathophysiological alterations in ventilation, perfusion and ventilation-perfusion matching along with respiratory mechanics. Characterization of these fundamental aspects of metabolic disorders, such as obesity and diabetes, present major public health concerns, and pose a global challenge for health care providers (76-78). Type 2 diabetes (T2DM) is the largest subtype (90% to 95%) and is a consequence of relative or absolute insulin deficiency. The number of patients with diagnosed or undiagnosed diabetes requiring critical care management is continuously increasing, with incidence reaching 25% to 40%, and has continued to expand rapidly in the past decade (79-82). Therefore, there is a particular need for an increased awareness of diabetes in critically ill patients.

Pathologic metabolic processes lead to endothelial cell dysfunction, which is caused by increased oxidative stress (83), and result in an imbalance between constrictor and dilator mechanisms that are characterized by overexpression of the vasoconstrictor endothelin-1 (ET-1) and diminished nitric oxide (NO) bioavailability and prostaglandin I_2 synthesis (80, 84, 85). Furthermore, persistent hyperglycaemia leads to an elevated level of advanced glycation end products (AGEs) (80, 81, 86, 87). In addition, the contractile tone of vascular smooth muscle is further elevated by direct mechanisms related to the Rho-kinase pathway, resulting in increased phosphorylation of myosin light chains (79, 88). All these cellular mechanisms manifest at an organ level as increased apoptosis, vascular permeability, vascular tone, extracellular matrix proliferation, and prothrombotic and proinflammatory tendencies (79-81, 83-86).

These pathophysiological changes are also expected to affect the lungs. The endocrine and paracrine consequences of endothelial dysfunction may trigger airway and lung parenchymal remodelling related to AGEs, oxidative stress, imbalance between NO and ET-1 pathways, and decreased prostaglandin I_2 level (81, 84, 86). All these processes may contribute to deterioration of lung function at the organ level (89). Since the pulmonary vessels and extracellular matrix cells express glucose transporter 1 (90), glucose influx from the blood to the interstitium is not limited.

In an attempt to clarify the pulmonary effects of diabetes, spirometric studies have revealed deteriorations in lung function indices (91-94). Nevertheless, lack of detrimental changes in

spirometric outcomes was also reported (95-98). The well-established methodological limitation of spirometry (99, 100) and the substantial differences among study populations (e.g., type and severity of diabetes, age and comorbidities) may have contributed to this discrepancy. Furthermore, the effect of obesity as a potential confounding factor was not assessed separately, and this may have further confused the findings.

AIMS AND HYPOTHESES

Studies included in the present thesis were designed to verify the use of capnography and extend its indications field in special patient groups and/or unique clinical situations. We characterized the ability of capnography to support clinical decision-making about the optimization of ventilator facilities during the outbreak of COVID-19 pandemic or in other catastrophic situations, such as combat casualty care. Furthermore, we also sought to investigate whether capnography contributes to revealing novel information about the cardiopulmonary status of a ventilated patient with metabolic disorders. Accordingly, the specific aims of the present thesis can be defined as follows.

Study I.:

To establish the use of capnography to verify emergency ventilator sharing in the COVID-19 era by

i) testing the use of capnography as a simple, noninvasive, online and goal-oriented bedside method for controlling the adequacy of split ventilation in each patient,
ii) investigating the presence of potential collateral gas flow between the two lungs with different time constants, and
iii) offering a simulation-based algorithm for ensuring equal tidal volumes by counterbalancing the difference in compliances by adjusting the resistance on the contralateral side.

Study II.:

To assess similarities and differences in the alterations of respiratory mechanics and gas exchange abnormalities in metabolic disorders by

i) characterizing the effects of diabetes and obesity separately on the airway function and viscoelastic properties of the respiratory tissues,
ii) establishing how diabetes alone would affect ventilation heterogeneity, ventilation–perfusion matching, and gas exchange in cardiac surgery patients, with particular focus on the applicability of the findings in intensive care clinical practice.

MATERIALS AND METHODS

Study I.: Use of capnography to verify emergency ventilator sharing in the COVID-19 era

Ethical approval was not necessary in this bench-test study, as no data of animal or human origin were considered.

The experimental setup

The experimental setup is shown schematically in Figure 3. Testing apparatus included two symmetrical model lungs. The model on each side was built from a 7-mm inner diameter commercial endotracheal tube to mimic the airways, and a commercially available artificial lung (type VA8001, Great Group Medical Co., Ltd., Taiwan) to represent compliant respiratory tissues. This double-lung system was ventilated with a commercially used ventilator (Dräger Evita XL, Dräger Medical, Lübeck, Germany). The ventilator circuit was divided symmetrically into two inspiratory and expiratory limbs by introducing Y-piece connectors close to the inlet and outlet ports of the ventilator. The length of each limb was 110 cm.

Two mainstream capnographs (Capnogard 1265, Novametrix, Andover, MA, USA) were connected to each circuit. The airflow (V') on each side was measured by a 11-mm internal diameter pneumotachograph (PNT Series, Hans Rudolph, Shawnee, KS, USA) connected to a miniature differential pressure transducer (24PCE-FA6D Honeywell, Charlotte, NC, USA). The pressure inside each model lung respectively was measured via connecting identical pressure sensors (24PCE-FA6D Honeywell, Charlotte, NC, USA) to the lateral ports. A rubber band was used on one side referred as Low C to decrease the compliance, whereas a Hoffmann clamp was placed around the endotracheal tube on the contralateral side referred as High R.

Plastic tubing was attached to the apex of each test lung allowing a seal-proof carbon dioxide (CO_2) gas inflow from a CO_2 reservoir bag supplied by a medical CO_2 cylinder. To ensure identical amount of CO_2 delivery into each side, a roller pump (Terumo Sarns 9000 Heart-Lung Machine, Terumo Europe NV, Leuven Belgium) was used as a flow generator to feed the CO_2 tubing system divided with a T-piece with an on-off clamp on each side. This system guaranteed the delivery of the same CO_2 concentration alternately even if the impedance of the artificial lung is varied depending on the applied elastic and/or resistive load. This setup mimics physiological CO_2 production with a constant rate of 200 ml/min. The CO_2 delivery system also enabled monitoring the adequacy of ventilation via measuring the end-tidal partial pressure

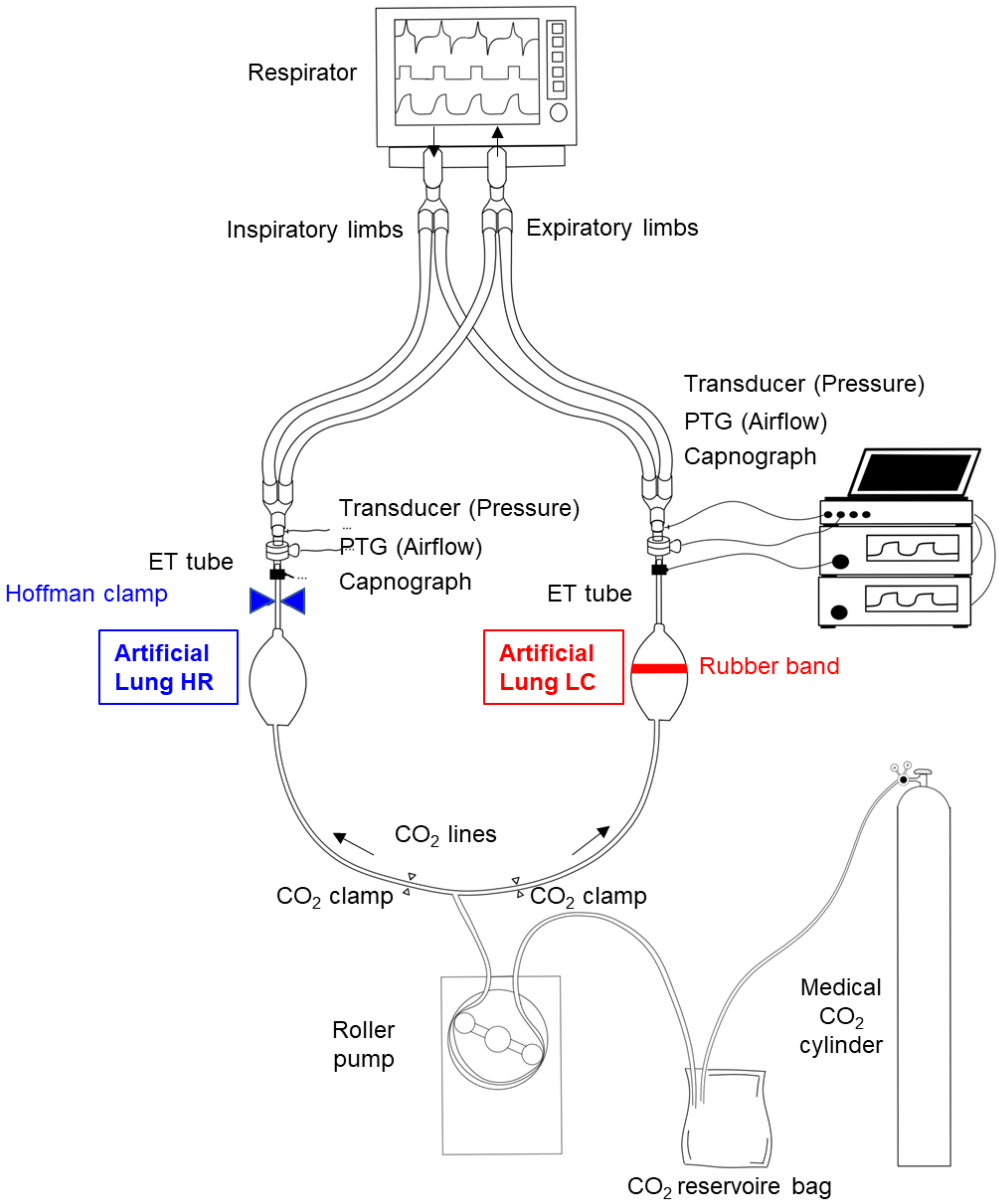

Figure 3. *Scheme of the experimental setup for ventilation sharing.*

The inspiratory and expiratory limbs connected to the ventilator were divided into two symmetrical pathways. Both inspiratory and expiratory tubing were connected after the inspiratory and before the expiratory valves of the respirator, respectively. Two identical systems were used to measure CO_2 concentration, pressure was measured by using pressure transducers via lateral ports ("Transducer (Pressure)"), and airflow was sensed by calibrated screen pneumotachographs ("PTG (Airflow)") in each artificial lung. The controlled CO_2 inflow into each model lung side was standardized by using a flow generator connected via tubing equipped with CO_2 clamps. Only one of the CO_2 clamps was open during the capnography measurements to avoid uneven distribution of CO_2 flow into each lung side depending on the load impedance. The model lung with red rubber band represents low compliance side, while the model lung with blue Hoffman clamp denotes the increased resistance. Lung HR: high resistance lung side, Lung LC: low-compliance lung side.

of CO_2 on each side, respectively. In addition, unilateral CO_2 delivery combined with bilateral capnography allows the assessment of the potential collateral gas flow between the two lungs with different time constants.

Data acquisition

Data epochs containing 30-s registrations of airflow and pressure signals of each test lung were digitized at a sampling rate of 256 Hz and recorded via a custom-made data acquisition software. The time-series datasets were analysed by using the LabChart software (version 7, ADInstruments, Sydney, Australia). The peak inspiratory (PIF) and expiratory flow rates (PEF), and the peak inspiratory pressure (Ppi) were determined via peak analyses. Tidal volumes (V_T) for each lung were calculated by integrating the corresponding V' signals. Respiratory parameters characterising both lungs together were registered from the display of the respirator. Values of VT, PIF, PEF, Ppi and $PetCO_2$ were averaged over the 30-s measurement period; since the bench test results were highly reproducible, the scatters in the parameters were negligible (coefficient of variation <0.7%).

Simulation study

A mathematical simulation study was performed to assess the magnitude of the resistance necessary to counterbalance the decreased compliance on the contralateral side to meet the clinical need of delivering equal tidal volumes to both patients connected to the splitted ventilation circuit. The simulation was based on the postulation that equal tidal volumes are delivered to both lungs if the absolute values of the loading impedances are identical, even if the resistive and elastic components are different on the two sides:

$$|Z_{LC}| = |Z_{HR}| \quad (1)$$

Indexes LC and HR refer to low compliance (Low C) and high resistance (High R) lung sides, respectively. Considering that the total respiratory impedance contains a real part (R) representing the resistive, and an imaginary part (X) reflecting the elastic components, equation (1) can be written as:

$$R_{LC}^2 + X_{LC}^2 = R_{HR}^2 + X_{HR}^2 \quad (2)$$

The real parts can be represented by single resistance values, while the X is inversely related to compliance ($X=1/(2\pi fC)$), where f is the ventilation frequency). The resistance needed to counterbalance the decreased compliance on the contralateral side can be expressed as:

$$R_{HR} = \sqrt{R_{LC}^2 + \left(\frac{1}{2\pi f C_{LC}}\right)^2 - \left(\frac{1}{2\pi f C_{HR}}\right)^2} \qquad (3)$$

The simulation assumed equal initial resistance on both sides with values encountered commonly in clinical practice, by using 8 $cmH_2O.s/l$ as physiological value (101) and 12 $cmH_2O.s/l$ as moderately elevated total respiratory resistance. The compliance was considered highly variable between two simulated patients, since virus pneumonia in COVID-19 compromises primarily the lung distensibility (66, 67).

Measurement protocol

The first set of data were collected in a system with intact test lungs possessing identical compliance and resistance parameters. Under this baseline condition (BL), volume-control mode with decelerating flow (Drager Autoflow®) was applied with a total V_T of 840 ml divided into 420 ml on each side. The end-expiratory pressure (PEEP) was set to 5 cmH_2O and the resulting Ppi was 22 cmH_2O. Mechanical parameters of ventilation (V_T, PIF, PEF and Ppi) were measured in parallel for each lung side. $PetCO_2$ values were registered alternately in each lung by clamping the contralateral limb of CO_2 tubing to avoid shunting of CO_2 delivery to the lung side with lower loading impedance. After completing these baseline measurements, the compliance was compromised with placing the elastic rubber band around one of the test lungs. In this unilateral low-compliance condition (LC), the same measurements were carried out as in condition BL. To counterbalance the decreased compliance on the low compliance side, the resistance was then adjusted with the Hoffmann clamp on the opposite high resistance side, and the same measurement sequence was repeated in this high-resistance condition (HR) as in the BL stage.

The ventilation was then changed to pressure-controlled mode. The pressure control level was set to maintain the same V_T as in the volume-control mode, i.e., 22 cmH_2O. Another set of BL data with symmetrical lungs and under Low C condition were then collected identical to the volume-control mode. In the third phase of the measurement when high compliance on one side was associated with high resistance on the other side, the pressure control level was elevated to 29 cmH_2O to provide physiological V_T and $PetCO_2$ in both model lungs.

Study II.: Obesity and diabetes: similar respiratory mechanical, but different gas exchange abnormalities

Ethical considerations

The study protocol was approved by the Human Research Ethics Committee of University of Szeged, Hungary (no. WHO 2788), and the patients gave their informed consent to participate in the study. The study was performed in accordance with the ethical standards laid down in the 1964 Declaration of Helsinki and its later amendments. The study followed the applicable CONSORT guidelines, and the patient flow chart is shown in Figure 4.

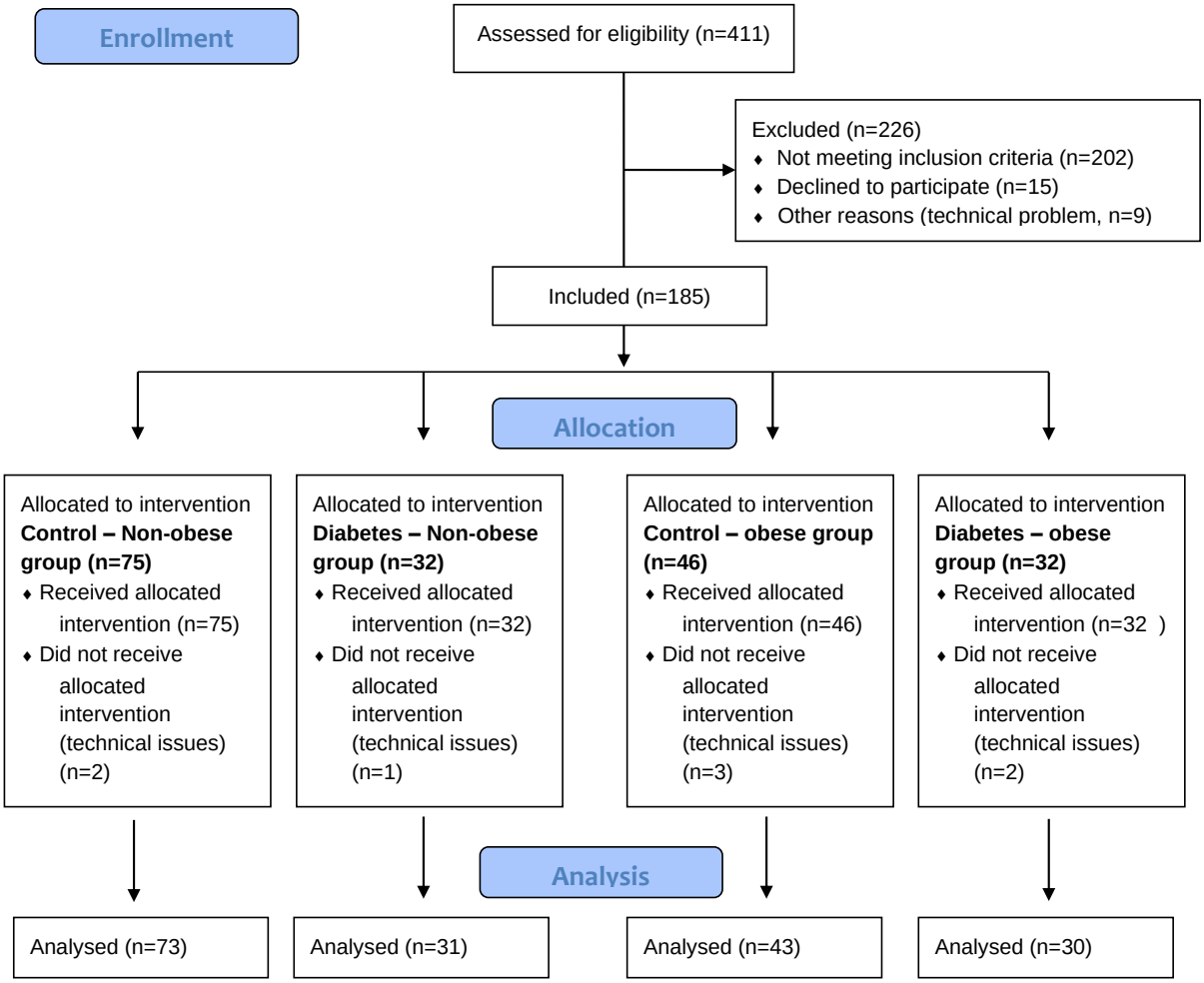

Figure 4. *Patient flow chart for Study II.*

Patients and study groups

This was a prospective study that enrolled 177 patients who underwent elective cardiac surgery (trial registration No. NCT03768973). Patients were assigned into four groups based on the metabolic status. Study subjects with body mass index (BMI) <30 kg/m^2 were divided into the control non-diabetic (C-N, n = 73) and diabetic (D-N, n = 31) groups. Obese patients (BMI ≥ 30 kg/m^2) were divided according to the presence (D-O, n = 30) or absence (C-O, n = 43) of diabetes. T2DM was defined if the medical history of the patient included a diagnosis of T2DM and/ or the haemoglobin A1c (HbA1c) level was >6.4%. The following exclusion criteria were applied for this study: older than 80 years of age, poor ejection fraction (<40%), and medical history of smoking or chronic obstructive pulmonary disease (COPD).

Anaesthesia and patient monitoring

One hour before the surgery, patients were premedicated with lorazepam (*per os,* 2.5 mg). Anaesthesia was induced by intravenous (iv) administration of midazolam (30 μg/kg), sufentanil (0.4–0.5 μg/kg), and propofol (0.3–0.5 mg/kg) and was maintained with iv propofol (50 μg/kg/min). Neuromuscular blockade was ensured by intravenous boluses of rocuronium (0.8 mg/kg for induction and 0.2 mg/kg every 30 minutes for maintenance). Endotracheal intubation was performed using a cuffed endotracheal (ET) tube with an internal diameter of 7, 8, or 9 mm. Patients were mechanically ventilated (Dräger Zeus, Lübeck, Germany) in volume-controlled mode with a tidal volume of 7 ml/kg and a positive end-expiratory pressure of 4 cmH_2O with decelerating flow. The ventilation frequency was adjusted to 12–14 breaths/min to achieve an end-tidal carbon dioxide partial pressure of 36–40 mmHg and the fraction of inspired oxygen was maintained at 0.5 during the study period. As a standard part of the cardiac anaesthesia procedure, oesophageal and rectal temperature probes were introduced, and a central venous line was secured in the right jugular vein. The left radial artery was also cannulated for monitoring systolic, diastolic and mean arterial blood pressures and taking arterial blood gas samples.

Recording and analyses of the volumetric capnogram

Changes in the CO_2 partial pressure in the exhaled gas during mechanical ventilation were measured with a calibrated mainstream capnograph (Capnogard Model 1265, Novametrix, Andover, MA). The measured 15-second long signals were digitized at a sampling rate of 102.4

Hz, stored on a computer and analysed with a custom-made software, as detailed previously (8).

The slopes of phase III of the time (S3T) and volumetric (S3V) capnograms were determined by fitting a linear regression line to the last 60% of phase 3 both on the time and volumetric capnograms, respectively (8). S3T expresses the change in in the partial CO_2 pressure of the exhaled gas per unit time [mmHg/s] and S3V per unit in the exhaled gas volume (mmHg/l).

Ventilation dead space parameters were calculated from the volumetric capnograms, and their values were related to the V_T. The anatomical dead space according to Fowler (V_{DF}), the physiological dead space according to Bohr (V_{DB}), and Enghoff dead space (V_{DE}) were calculated as described above. Difference between V_{DE}-V_{DB} were calculated as a surrogate of the intrapulmonary shunt.

Measurement protocol

Before starting the surgical procedure, the measurements were carried out on the mechanically ventilated patients under general anaesthesia and muscle relaxants. After securing the invasive and non-invasive monitoring equipment, lung recruitment was performed to standardize the volume history by inflating the lungs to an intratracheal pressure of 30 cmH_2O. A five-minute period was then allowed to reach steady-state hemodynamic and respiratory mechanical conditions while the PEEP was maintained at a level of 4 cmH_2O. Arterial and central venous blood gas samples were taken, and the R and C were registered from the display of the respirator. Registration of at least two technically acceptable capnogram curves in 1 min intervals was also performed.

Statistical analyses

For numerically reported data, the scatters in the measured variables are expressed as the half width of the 95% confidence interval for the mean. The normality of the data was tested with the Shapiro–Wilk test. Two-way analysis of variance (ANOVA) with factors of diabetes and obesity was used to assess the effects of these disorders on the measured variables. The Holm–Sidak multiple comparison method was used to test pairwise differences between the protocol groups. Sample sizes were estimated to enable detection of a clinically relevant 25% difference in the primary outcome parameter, the airway resistance. Accordingly, sample size estimation based on an ANOVA test with four groups of patients indicated that at least 28 patients were

required in each group to detect a statistically significant difference between the protocol groups, with assumed variability of 10%, power of 80%, and a significance level of 5%. The statistical tests were performed with a SigmaPlot statistical software package (Version 13, Systat Software, Inc. Chicago, IL, USA), with a significance level of $p < 0.05$. All reported p values were two-sided.

RESULTS

Study I.: Use of capnography to verify emergency ventilator sharing in the COVID-19 era

Table 1. summarizes the resistance, compliance parameters displayed by the ventilator during the measurements in volume- (VC) and pressure-controlled (PC) ventilation modes, and the calculated time constant ($\tau = R \cdot C$). Readings were made under baseline conditions (BL), after unilateral decrease in compliance (LC) and contralateral compensation with high resistance (LC + HR). To assess the level of asymmetry in the mechanical parameters, individual compliance values were calculated by using the measured individual tidal volumes and distending pressures on each side. Estimation of individual resistances characterizing each side were based on equation (3).

		R_{LowC}	R_{HighR}	R	C_{LowC}	C_{HighR}	C	τ_{LowC}	τ_{HighR}
VC	**BL**	*17.4*	*17.4*	8.7	*33*	*33*	65	*0.57*	*0.57*
	LC	*18.2*	*18.2*	9.1	*20*	*34*	54	*0.36*	*0.63*
	LC + HR	*17.4*	*40.7*	12.2	*18*	*31*	49	*0.31*	*1.27*
PC	**BL**	*17.4*	*17.4*	8.7	*33*	*33*	65	*0.57*	*0.57*
	LC	*18.2*	*18.2*	9.1	*20*	*35*	55	*0.36*	*0.64*
	LC + HR	*17.4*	*39.5*	12.1	*18*	*33*	51	*0.32*	*1.28*

Table 1. *Mechanical parameters obtained during ventilator sharing.*
Resistance, compliance parameters displayed by the ventilator (R and C) and time constant ($\tau = R \cdot C$) under baseline conditions (BL), after unilateral decrease in compliance (LC) and contralateral compensation with high resistance (LC + HR) in volume- (VC) and pressure-controlled (PC) ventilation modes. Calculation of individual compliance values were based on the measured tidal volumes and distending pressures on each side. Calculation of individual resistances are based on equation (3). R and C values are expressed in $cmH_2O.s/l$ and ml/cmH_2O, respectively. τ is in seconds. Normal fonts: measured parameters, italic fonts: calculated parameters.

Representative volume, capnogram, airflow and pressure curves are illustrated on Figure 5. Under baseline conditions, the curves obtained on two lung sides overlap, indicating no difference in the mechanical properties between the two test lungs. After compromising the compliance unilaterally (condition LC), the reduced VT on the stiffer lung side was associated with an increased VT on the other side without intervention. Consequently, the $PetCO_2$ became higher in the lung with low compliance and reduced on the reference side. Following the

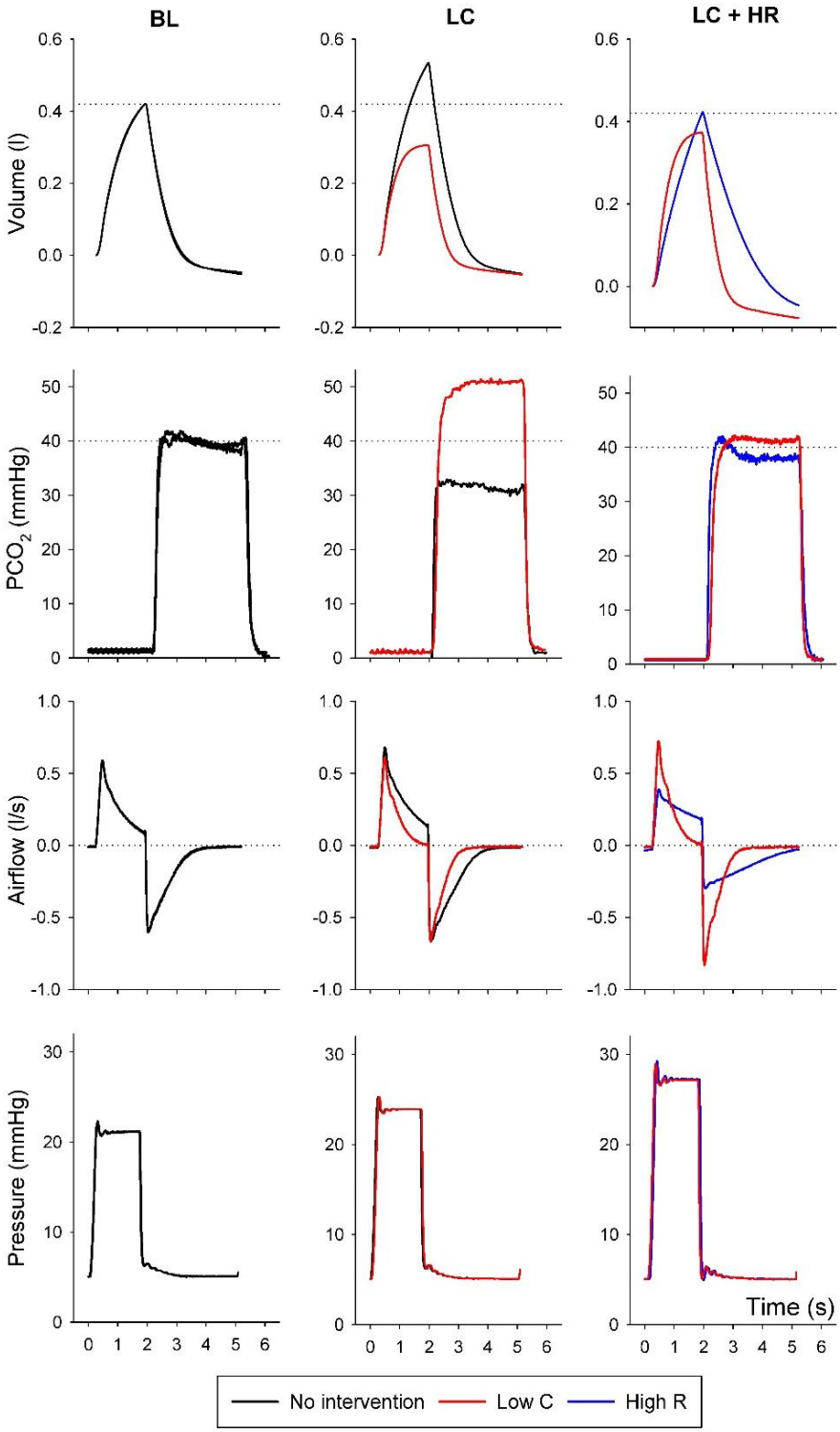

Figure 5. *Representative volume, capnogram (PCO_2), airflow and pressure curves.*
Data were obtained under baseline condition (left panels), during unilateral decreased compliance (middle panels) and following the compensation of unilaterally decreased compliance with contralateral high resistance (right panels) during volume-controlled ventilation. Black curves represent no intervention, red curves reflect low compliance side (Low C), blue curves denote high resistance side (High R).

contralateral elevation of resistance, the V_T and $PetCO_2$ values were re-equilibrated, whereas the flow pattern exhibited marked differences with restrictive and obstructive flow patterns on the Low C and High R sides, respectively. The plateau pressure levels elevated stepwise after each intervention, with no difference between the two communicating sides.

The average values of the main outcome parameters are summarized on Figure 6. Under baseline conditions (BL), the V_T was equally distributed between the two model lungs, with no difference between the capnographic and mechanical parameters both in volume- and pressure-control modes. The unilateral decrease in compliance in volume control mode resulted in an uneven distribution of V_Ts with lower volume on the interventional side and elevated V_T on the intact model lung. These volume differences were also manifested in the $PetCO_2$ asymmetry. The decrease in global compliance caused elevations in Ppi equally on both sides. Unilateral stiffening during pressure-control ventilation decreased V_T and increased $PetCO_2$ on the restricted side, whereas the intact side remained at the baseline level determined by the constant driving pressure level. Counterbalancing the lung restriction contralaterally with an increased flow resistance redirected the ventilation to the stiffer lung. This intervention led to different airflow profiles between the two sides (PIF, PEF) redistributing the mechanical ventilation as evidenced by the normalized V_T and $PetCO_2$ levels on both sides. These effects are uniform in volume- and pressure-controlled ventilation modes, however the Ppi need to be increased intentionally in pressure-controlled mode.

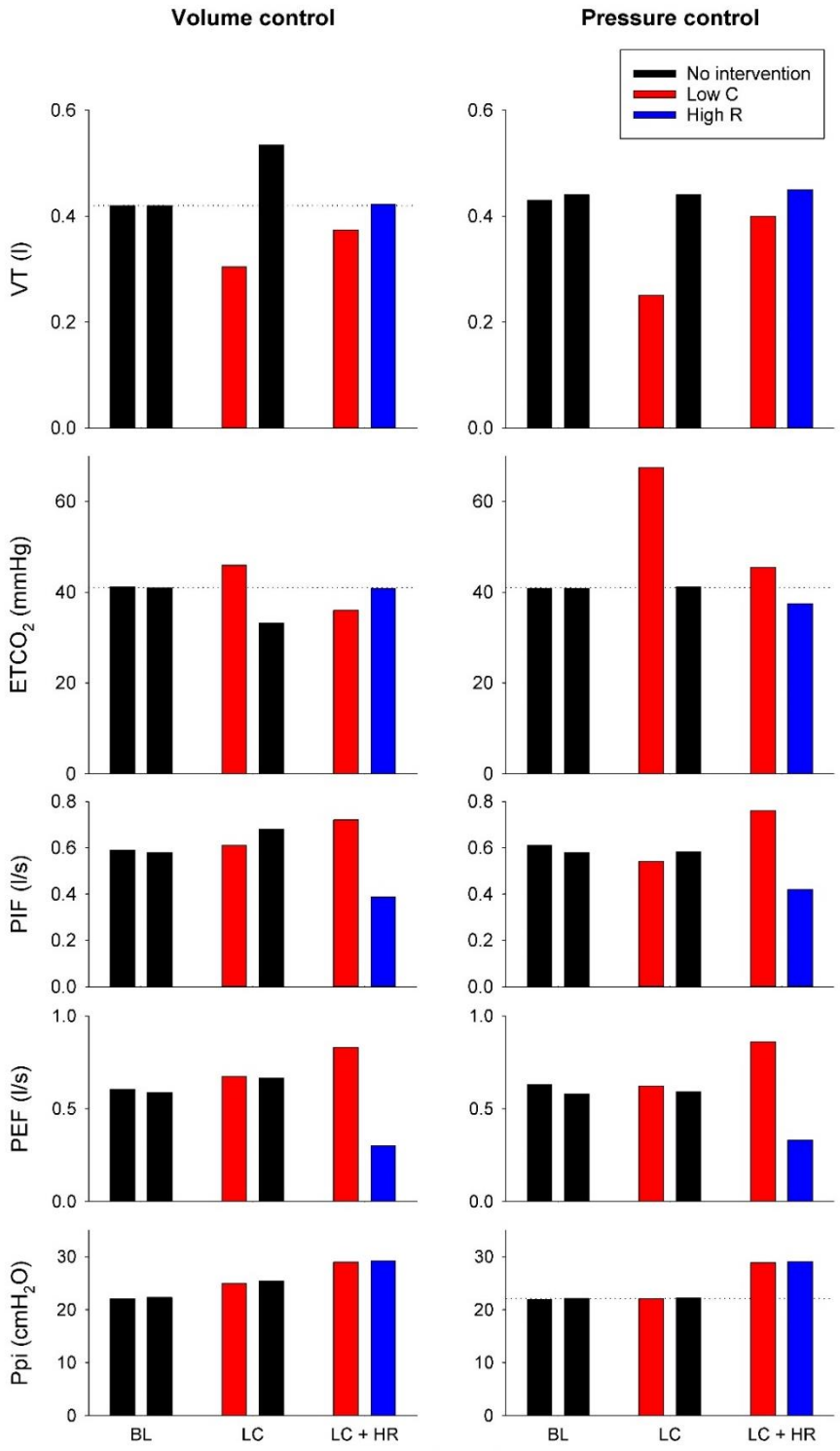

Figure 6. *Ventilation parameters obtained in ventilator sharing.*

Tidal volume (VT), end-tidal CO_2 concentration ($ETCO_2$), peak inspiratory- (PIP) and expiratory flows (PEF) and peak inspiratory pressure (Ppi) obtained by averaging the 30-s long recordings under volume- (left) and pressure-controlled (right) ventilations. Black bars represent no intervention, red curves reflect low compliance side (Low C), blue curves denote high resistance side (High R). Results were obtained under baseline conditions (BL), after unilateral decrease in compliance (LC) and contralateral compensation with high resistance (LC + HR).

The results of the mathematical simulation study are demonstrated on Figure 7. by assuming normal (left) and elevated (right) total respiratory resistance levels. The graphs show the resistance values necessary to counterbalance the asymmetry in compliance values to deliver the same tidal volumes to both patients connected to the split ventilation circuit. The compliance values of the two ventilated sides are indicated on the labelled curves and the x-axes, and the targeted contralateral resistance values can be read from the y-axes.

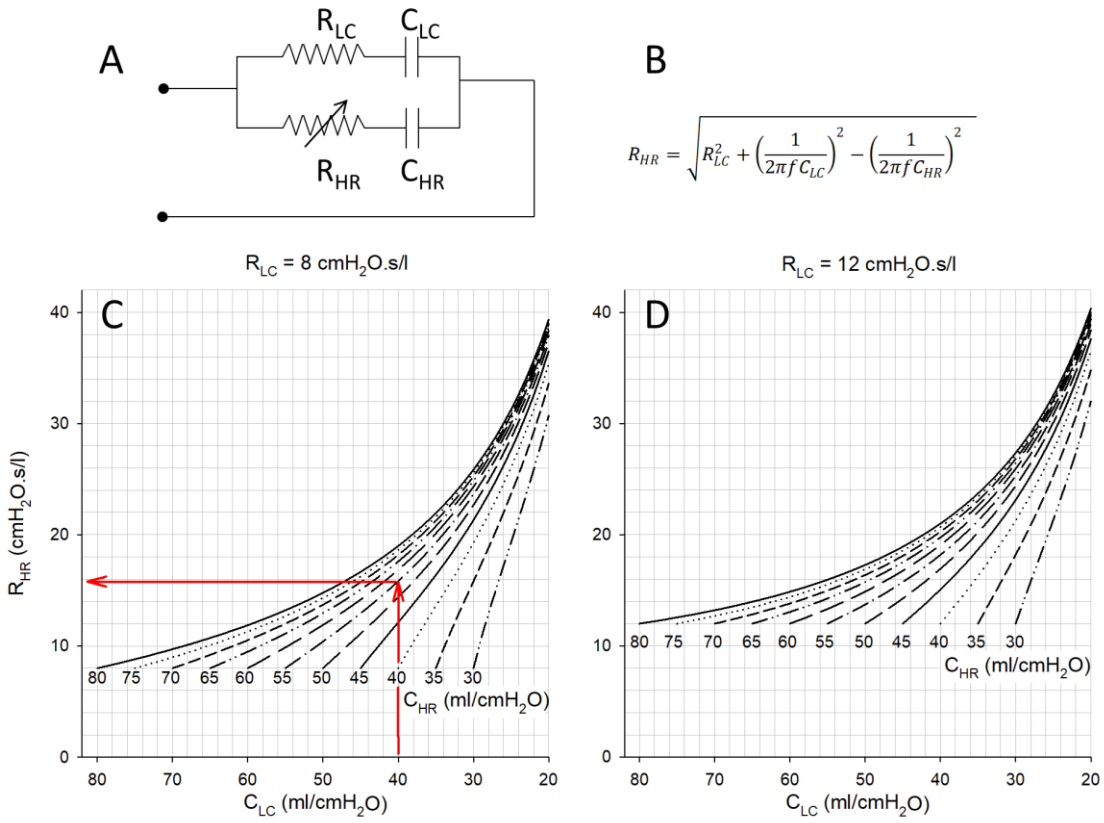

Figure 7. *Results obtained from the simulation study.*

The shared ventilation system is modelled by parallel connection of single compartment respiratory system impedances including resistance and compliance. Panel B: equation to calculate the compensatory resistance to equalize different impedances. Results of the mathematical simulation study with setting physiological (Panel C) and moderately elevated (Panel D) total respiratory resistance levels on the low-compliance side (RLC). The nomograms with different curves show the resistance values necessary to counterbalance the asymmetry in compliance values to deliver the same tidal volumes to both sides of a split ventilation circuit. The compliance values of the two ventilated sides are indicated on the labelled curves (CHR) and the x-axis (CLC), respectively. The targeted contralateral resistance values are obtained from the y-axis. Red arrows indicate a particular example: a resistance value of 14.9 cmH_2O.s/l (RHR) is necessary to counterbalance the compliance asymmetry if the resistance and compliance on the low compliance side is 8 cmH_2O.s/l (RLC) and 40 mL/cmH_2O (CLC), respectively, and the compliance on the contralateral side is 55 mL/cmH_2O (CHR).

Study II.: obesity and diabetes: similar respiratory mechanical, but different gas exchange abnormalities

Table 2. summarises the demographic, anthropometric and the main clinical characteristics of the patients in the four protocol groups. The study groups had no differences in height, age, and ejection fraction. As expected, body weight and body mass index (BMI) were significantly higher in the obese patients than in non-obese patients ($p < 0.001$). Elevated levels of serum glucose ($p < 0.001$) and HbA1c ($p < 0.001$) were observed in patients with diabetes.

	Group C-N (n = 73)	**Group D-N (n = 31)**	**Group C-O (n = 43)**	**Group D-O (n = 30)**	***p***
Weight (kg)	71.4 ± 12.9	74.0 ± 9.1	97.2 ± 17.1	93.3 ± 16.1	<0.001
Height (cm)	167.3 ± 8.9	168.0 ± 6.2	167.7 ± 11.5	162.6 ± 6.2	0.088
BMI (kg/m^2)	25.4 ± 0.8	26.1 ± 1.2	34.0 ± 1.2	35.6 ± 1.7	<0.001
Age (years)	68.2 ± 10.9	69.9 ± 7.3	67.1 ± 10.7	69.9 ± 7.4	0.53
Ejection fraction (%)	62.2 ± 6.1	60.1 ± 7.4	61.9 ± 6.4	59.2 ± 7.6	0.14
Glucose (mmol/L)	6.17 ± 1.1	8.62 ± 3.36	6.65 ± 1.66	8.16 ± 2.92	<0.001
HbA1c (%)	5.63 ± 0.37	7.12 ± 1.39	5.62 ± 0.43	7.19 ± 1.06	<0.001
Duration of T2DM (years)	-	9.5 ± 8.5	-	11.0 ± 8.8	0.5

Table 2. *Patient characteristics.*
Parameters are presented for the protocol groups C–N: no diabetes, no obesity; D–N: diabetes, no obesity, C–O: no diabetes, obesity; D–O: diabetes, obesity; HbA1c: Hemoglobin-A1c. BMI: body mass index

The resistance and compliance parameters obtained in the protocol groups are summarised in Fig. 8. Diabetes had no statistically significant effect on R regardless of the presence of obesity. However, obesity elevated R significantly in the patients without diabetes (p<0.005), with no

such effect detectable in the presence of diabetes. Obesity caused significant diminishment of C in diabetic and non-diabetic patients ($p<0.005$ for both). Diabetes had a significant effect on C only in the patients without obesity ($p<0.005$).

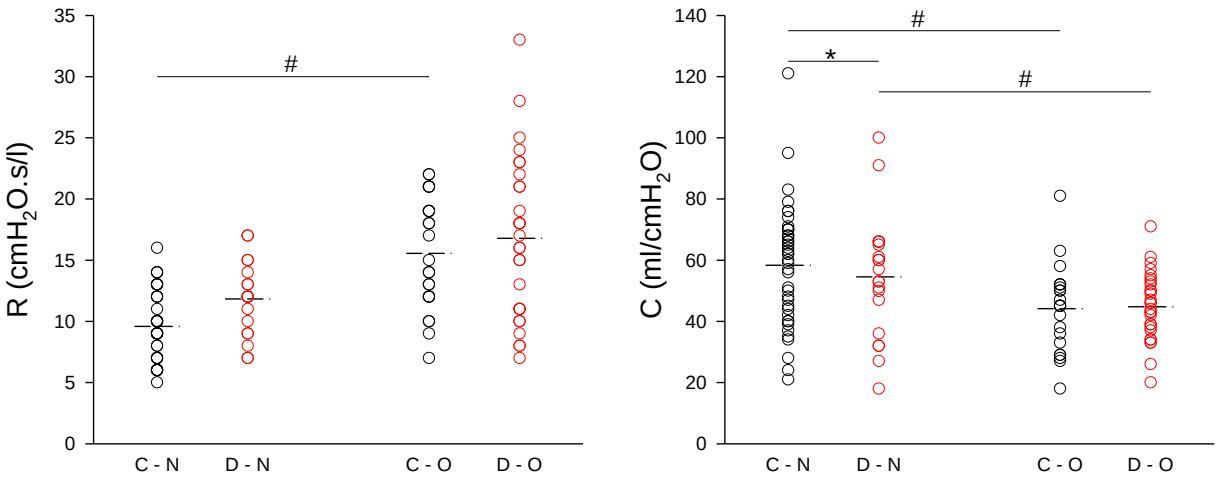

Figure 8. *Respiratory mechanical data in patients with diabetes and/or obesity.*
*Resistance (left) and compliance parameters (right) obtained in patients without (C) and with (D) type 2 diabetes mellitus associated with normal body shape (N) or obesity (O). C–N: no diabetes, no obesity; D–N: diabetes, no obesity, C–O: no diabetes, obesity; D–O: diabetes, obesity. *: p<0.05 for diabetes; #: p<0.05 for obesity*

Shape factor and dead space parameters obtained by capnography in the four protocol groups are demonstrated in Fig. 9. Significantly elevated levels of S3T and S3V were obtained for patients with T2DM alone ($p < 0.05$ for both). On the other hand, diabetes had no significant effects on the ventilation dead space parameters or intrapulmonary shunt (V_{DE}–V_{DB}). Both time domain and volumetric phase 3 slope parameters were significantly greater in obese patients than in non-obese patients ($p < 0.001$ for S3T and S3V), whereas V_{DF} ($p < 0.001$) and V_{DB} ($p < 0.001$) decreased with obesity. Obesity had no effect on the V_{DE}, but it significantly increased the V_{DE}–V_{DB} ($p < 0.005$).

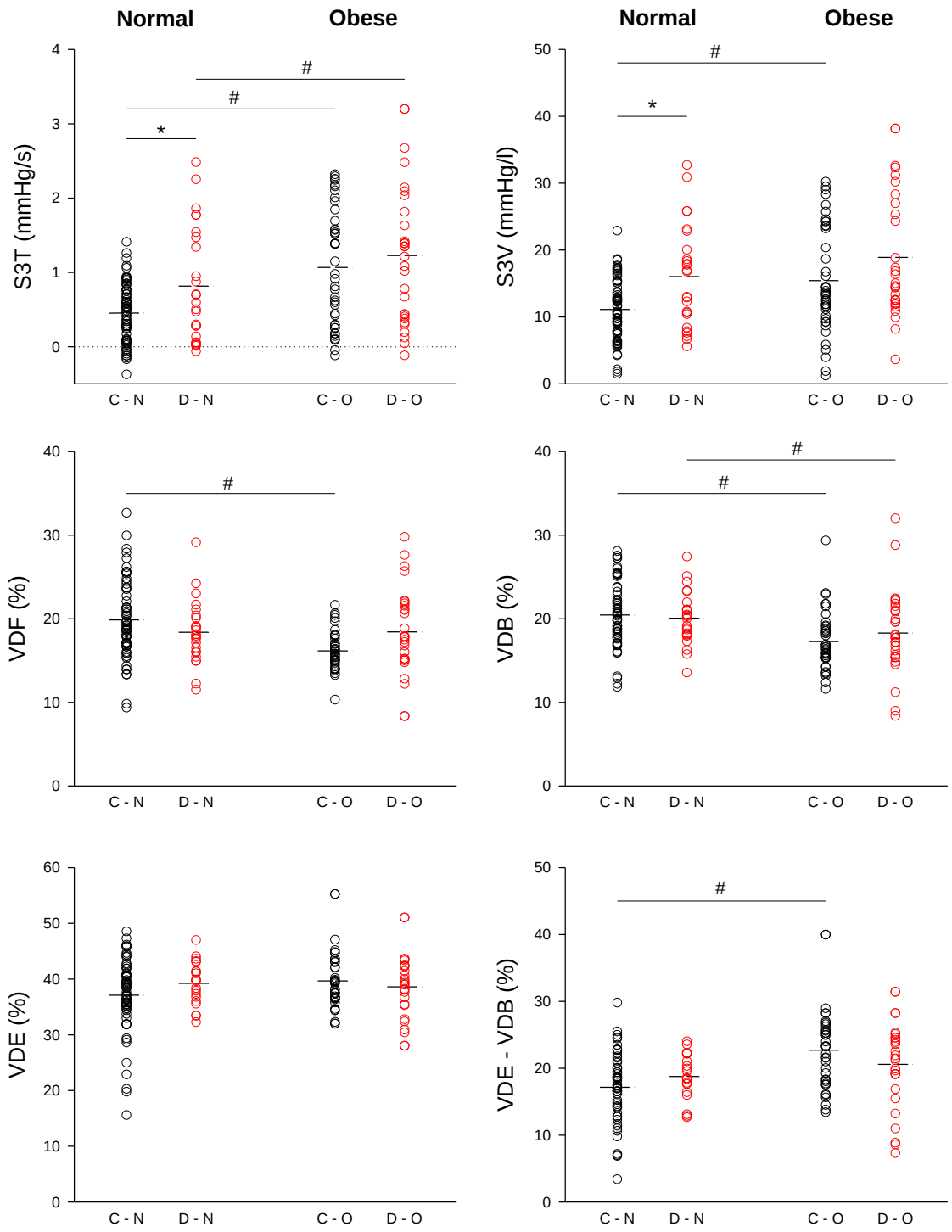

Figure 9. *Capnography data in patients with diabetes and/or obesity.*

*Phase 3 slope obtained by time (S3T) and volumetric (S3V) capnography, ventilation dead space fractions relative to the tidal volume according to Fowler (VDF), Bohr (VDB) and Enghoff (VDE), and the intrapulmonary shunt assessed as VDE–VDB. Capnographic outcomes were obtained in patients without (C) and with (D) type 2 diabetes mellitus associated with normal body shape (N) or obesity (O). C–N: no diabetes, no obesity; D–N: diabetes, no obesity, C–O: no diabetes, obesity; D–O: diabetes, obesity. *: p<0.05 for diabetes; #: p<0.05 for obesity.*

The gas exchange parameters in the four protocol groups are depicted in Fig. 10. The presence of diabetes had no significant effects on PaO_2/FiO_2 and Qs/Qt. Conversely, obesity significantly diminished PaO_2/FiO_2 and Qs/Qt ($p < 0.001$ for both).

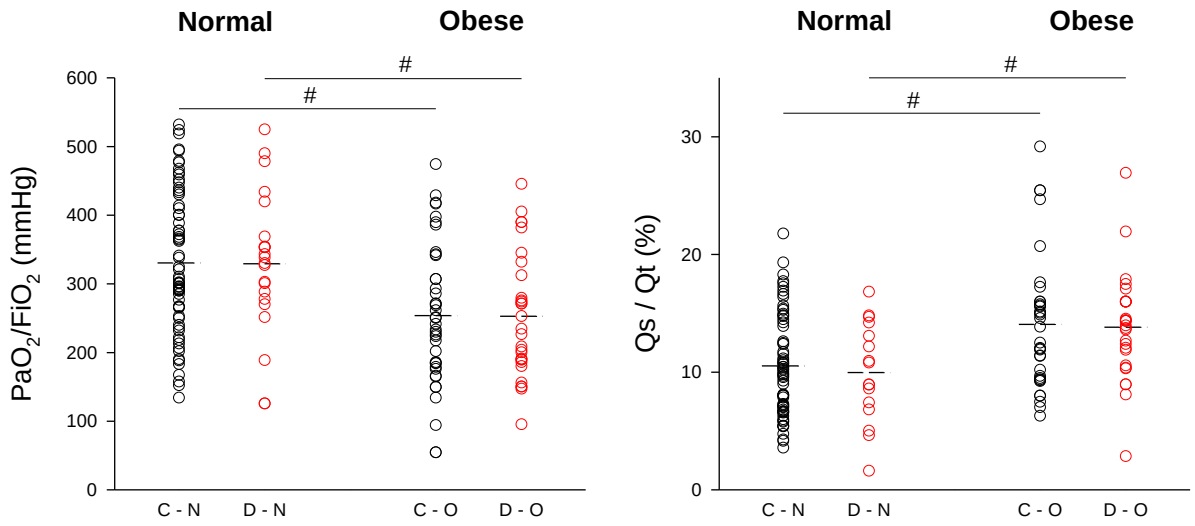

Figure 10. *Gas exchange data in patients with diabetes and/or obesity.*
*Parameters were obtained in patients without (C) and with (D) type 2 diabetes mellitus associated with normal body shape (N) or obesity (O). PaO_2/FiO_2: lung oxygenation index, Qs/Qt: intrapulmonary shunt obtained by the Berggren equation. C–N: no diabetes, no obesity; D–N: diabetes, no obesity, C–O: no diabetes, obesity; D–O: diabetes, obesity. *: p<0.05 for diabetes; #: p<0.05 for obesity*

DISCUSSION

Beyond the well-established indications of capnography in airway and ventilation management, we extended the field of indication of this monitoring modality to unique emergency clinical situations as well as to reveal cardiorespiratory pathologies in diabetic and/or obese patient population. Our capnographic assessments demonstrated the potential for adequate gas exchange during emergent shared ventilation with no collateral airflow between the split sides, even in the case of great differences in mechanical load. In another study on a large cohort of mechanically ventilated patients, the separate effects of diabetes and obesity on lung ventilation and ventilation–perfusion matching were characterised. Diabetes had no effect on the total respiratory resistance and decreased respiratory system compliance. These mechanical abnormalities were associated with an elevated capnographic phase III slope. A remarkable finding of this study is that these adverse mechanical and ventilatory changes in diabetes did not result in pathologic gas exchange, in terms of ventilation dead space, intrapulmonary shunting or lung oxygenation index. Obesity caused similar detrimental

changes in respiratory mechanics and alveolar heterogeneity; however, these alterations were reflected in the compromised gas exchange.

Study I.: Use of capnography to verify emergency ventilator sharing in the COVID-19 era

Study I. was motivated by the potential risk of developing a shortage of ventilators in intensive care units in the pandemic period when the technical supply was not able to keep pace with the COVID-19 infection spread rate. This problem can also emerge in war situations when a sudden local increase may occur in the combat casualty care. In such an outbreak phase, clinicians may be faced with difficult decision making and a triage resulting from the mismatch in the number of patients requiring mechanical ventilation and the number of ventilators currently available (102-104). This clinical situation may ultimately require triaging and quick decision making. Aside from the clinical difficulties, serious ethical concerns may also arise, because viral pneumonia is not an incurable disease and ventilation support may be needed to bridge a temporal shortage of ventilators. The decision making is burdened by the lack of universal algorithms for triage, since the factors determining survival chances are highly variable. Furthermore, this decision in an emergency situation is likely to be based on incomplete information about the patient. Hence, it is reasonable to propose the concept of ventilator splitting as a lifesaving modality. A problem-oriented attitude motivated the concept of ventilator sharing as a life-saving manoeuvre, meaning that one apparatus may be used to ventilate multiple lungs.

However, ventilator splitting between two patients raises several concerns needing clarification before this approach can be considered in clinical settings. A notable challenge arises from the fact, that the simultaneously ventilated individuals may differ in their respiratory mechanics due to the asymmetry in anthropologic features and/or severity of their respiratory symptoms. The feasibility of solving this problem was recently demonstrated (74), where low compliance in one side was counterbalanced by an elevation of flow resistance contralaterally. In the current bench-test study, we also confirmed the validity of this concept. Given the fact that individual tidal volumes are distributed equally if the magnitude of the input impedances are equal, we offered a quick simulation-based algorithm for ensuring equal tidal volumes by overcoming differences in respiratory mechanics.

It is important to note, however, that the patients may differ in their metabolic rates and diffusion capacities. Thus, equal distribution of tidal volumes does not guarantee adequate

ventilation on both sides. Consequently, an additional monitoring modality is mandatory to verify the adequacy of ventilation in both individuals. Therefore, we implemented capnography as a simple, non-invasive, online and bedside method for controlling the adequacy of ventilation (16, 105). Since the expiratory capnogram reflects alveolar ventilation, capillary gas diffusion, and lung perfusion, this monitoring tool allows the assessment of the adequacy of ventilation individually in a goal-oriented manner (17). Indeed, the results of the present study confirmed that diminished V_T resulting from mechanical asymmetry was associated with hypercapnia in the low compliance side. This can be attributed to the maintained CO_2 production in a smaller gas compartment. Our findings demonstrate that capnography serves as a safe control modality to individualize the redirection of V_T into the stiffer side.

Ventilation with circuit splitting may generate a further concern related to the potential collateral bias flow between the patients. However, the pressure regimen during the ventilation cycle did not differ between the two sides independent of the ventilation mode. The lack of difference in the driving pressure at any point in time of expiration rules out the presence of collateral gas flow. The cross-breathing can also be excluded by the capnographic findings, i.e., there was no detectable CO_2 in one lung side when the CO_2 inflow was driven only into the other lung.

The compliance values of the model lungs with baseline compliance values of 27 ml/cmH_2O used in the current bench-test mimic diseased lungs restricted by virus pneumonitis. When asymmetry was generated, differences in the compliance values nearly doubled. This condition resembles to a split ventilation of a moderately and a severely injured lung. Redirection of airflow by increasing resistance on the higher compliance side compromised lung emptying, which was indicated by the distortion of the expiratory flow curve (Fig 5, LC+HR column, blue line). Following the application of this mechanical load, the flow pattern approached zero by the end expirations. Further need for such compensation in resistance may evoke incomplete lung emptying and thereby induce dynamic hyperinflation on the high-compliance high-resistance side. This finding points to the limitation of the volume-shifting methodology by unilateral resistance manipulation.

The results of this study also revealed the differences between the volume- and pressure-controlled ventilation modes to optimize ventilation parameters in a split system. In the case on volume-controlled ventilation, the opposite changes in V_T and $P_{ET}CO_2$ were observed between the two sides. However, using the pressure-controlled mode affected only the

manipulated side. It is of note that the pressure-control level determining the Ppi has to be elevated to counteract the resistive load used to shift V_T into the stiff side (Fig. 6, Ppi).

The limitations of Study I. also warrant discussion. For simplicity, in the mathematical simulation study, we considered close to normal or moderately elevated initial resistance values uniformly on both sides. As COVID-19 induces mainly restrictive changes indicated by moderately and severely compromised compliances (66, 67), asymmetry was generated in this mechanical parameter. A further simplification of the simulation model was related to the negligence of the dissipative energy loss in the respiratory tissues (101), which is expected to be elevated in this pathology. However, there is no data available currently to estimate the magnitude of alterations in this mechanical parameter. Even with these simplifications, the results of the simulations can serve as a starting point and the appropriateness of ventilation in each individual can be verified by capnography. A further methodological aspect of the present study is that simultaneous ventilation may only be feasible in a controlled mode, since the individual and different spontaneous activity cannot be synchronised between the two sides.

Study II. Obesity and diabetes: similar respiratory mechanical but different gas exchange defects

Study II. was motivated by the increasing number of diabetic and obese patients requiring surgical intervention with adequate and safe anaesthesia.

Effects of diabetes on respiratory function

While markedly increased airway resistance was obtained in patients with diabetes, regardless of the presence of obesity (18), this airway abnormality was not apparent from the global resistive parameter displayed by the ventilator (Fig. 8.). This seemingly controversial result can be explained by the involvement of significant components in R not specific to changes in airway geometry, such as flow-resistance of the ET-tube and the instrumental tubing, and resistance of the respiratory tissues (101). This result agrees with previous studies that demonstrated a decline in lung function indices obtained by spirometry (91-94) or plethysmography (95). Several mechanisms may contribute to this central airway abnormality, including excessive mucus production (106), activation of inflammatory pathways (107, 108), increased contractile tone or proliferation of airway smooth muscle cells (79, 109, 110) and/or diminished vagal tone (111). Involvement of the peripheral airways can be implied from elevations in the respiratory mechanical parameters reflecting enhanced ventilation

heterogeneities, phase 3 slopes obtained by time, and volumetric capnography. Increased Rho-associated kinase activity (79) and overexpression of α-smooth muscle actin (110), β-catenin (109), and/ or collagen (112) may be responsible for the increased contractile tone of bronchiolar smooth muscle cells, with the potential further involvement of the inflammatory pathways (107, 108, 113).

Interestingly, the deteriorations in respiratory mechanics in diabetic patients were not followed by adverse alterations in gas exchange parameters, such as ventilation dead space obtained by volumetric capnography (Fig. 9.), or in blood gas outcomes that reflect lung oxygenation and intrapulmonary shunting (Fig. 10.). The underlying mechanisms responsible for the maintained gas exchange despite the compromised respiratory mechanics were not entirely clear. Patients with diabetes are prone to enhanced general vasoconstrictive responses due to endothelial dysfunction (80, 81, 84-86, 113). This pathology is supposed to be present in an enhanced pulmonary vascular contractility in a hypoxic tissue environment (i.e., hypoxic pulmonary vasoconstriction). In this population, more rigorous and effective redirection of intrapulmonary blood into the ventilated lung regions may occur subsequently, thereby, reducing ventilation–perfusion mismatch. This relatively effective compensatory mechanism was supported by the lack of difference between the indices of intrapulmonary shunt expressed by capnography (V_{DE}–V_{DB}, Fig. 9.) and blood gas (Qs/Qt, Fig. 10.).

Effects of obesity on respiratory function

In the present study, obesity as a potential confounding factor was assessed separately from diabetes to gain distinct insights into the respiratory consequences of these common pathologies. This approach revealed identical direction and comparable magnitudes of changes in the respiratory mechanical parameters (R and C), and alveolar heterogeneity in obesity and diabetes. The respiratory mechanical changes in obesity were in accordance with previous results that demonstrated impaired respiratory resistance and tissue compliance (114, 115) and inhomogeneous lung emptying (19, 20) in obese patients. The underlying mechanisms responsible for such mechanical changes in obesity are markedly different from those in diabetes, and primarily involve the development of regional atelectasis and lung volume loss, which are caused by the external mechanical load exerted by the cranial displacement of the diaphragm.

Unlike in diabetes, the decline in respiratory mechanics in obesity was reflected in compromised gas exchange. The somewhat smaller anatomical dead space (V_{DF}) may be attributed to compression of the lung parenchyma, which leads to loss of gas volume in the conducting airways. The slightly reduced physiological (V_{DB}) dead space in obese patients can be explained by the cranial shift of the lung and the heart, resulting in possible reduction of lung regions with West I zones. Furthermore, the reduced PaO_2/FiO_2 in obese patients demonstrates the compromised oxygenation ability of the lung (Fig. 10.), which is consistent with abnormal pulmonary vascular contractility (116).

Some limitations of this clinical study warrant discussion. The patients involved in the present study underwent elective cardiac surgery, which may have affected the lung function outcomes. However, the distribution of heart diseases was homogenous among the protocol groups in this relatively large cohort of patients. Therefore, cardiopulmonary interactions were unlikely to have caused biases in the differences between the study groups. In addition, we made efforts to homogenize the study population in each group by excluding factors, such as smoking and COPD, which can affect basal lung function. This approach may have underestimated the real differences in the lung mechanical properties. However, measurements in intact chest conditions provide more valid representations of ventilation and ventilation–perfusion matching.

SUMMARY AND CONCLUSIONS

The extended application area of capnography was verified in a bench test study and clinical investigation.

The in vitro study involving artificial lungs with different mechanical properties gave insight into the uneven ventilation distribution driven by the markedly altered resistive and/or elastic properties of the individual sides. These findings contributed to a better understanding of ventilation heterogeneities in a lung, including compartments with different time constants.

Due to the high reproduction number of SARS-CoV-2 virus, there may be a sudden increase in the number of patients requiring mechanical ventilation. This can lead to an acute shortage of ventilators in critical care. Using capnogaphy in Study I., we demonstrated that the adequacy of ventilator splitting can be verified. However, ventilator splitting can only be considered as a rescue intervention to provide adequate tidal volumes without collateral airflow for two subjects with different respiratory systems. Our experimental results support that this split

ventilation modality can be applied without the risk of diminishing patient safety if emergencies arise due to temporal shortages of mechanical ventilators. Therefore, the risk of non-ventilation is higher than that of controlled shared ventilation in terms of morbidity. Moreover, goal-oriented capnography can serve as a bedside approach to ensure the adequacy of tidal volumes on both lungs during this life saving intervention. Capnography as a routinely available monitoring modality may help in emergencies (i.e., in pandemics or combat hospitals) when there is a lack of equipment and/or health care professionals. From this aspect, ventilator sharing can be regarded as a lifesaving manoeuvre in catastrophe medicine. This alternative may have importance during the exacerbation of an upcoming epidemic wave, or devastating war-related tragic events when intensive care specialists may be faced with a shortage of ventilators.

Study II. demonstrated that, diabetes affects airway function and the elastic properties of the respiratory tissues, leading to ventilation heterogeneities. This inhomogeneous alveolar emptying was confirmed by capnography showing an elevated phase III slope. These intrinsic mechanical and ventilation abnormalities in diabetes were counterbalanced by the increased contractile response of the pulmonary vasculature to hypoxic stimuli, which was able to maintain the normal intrapulmonary shunt fraction and oxygenation ability of the lungs. On the other hand, obesity similarly deteriorated the global respiratory mechanics, and the external trigger worsened gas exchange. The simultaneous presence of diabetes and obesity had additive effects on the worsened respiratory resistance. This synergistic effect may be related to the combination of the external mechanical overload exerted by the upward shift of the diaphragm in obesity, and the enhanced susceptibility of the alveoli to collapse subsequent to type II pneumocyte dysfunction in the presence of diabetes secretion. These pathophysiological changes highlight the importance of lung protective ventilation with high PEEP and low V_Ts not only in obesity, but also in patients with diabetes.

Taking together the findings of the two studies may have clinical relevance. Since a high proportion of the critically ill COVID-19 patients are diabetic and/or obese, detailed information obtained by capnography may help to optimize mechanical ventilation in the case of a necessity for shared ventilation in a population overwhelmed by diabetic and/or obese patients.

AKNOWLEDGEMENT

I would like to express my gratitude to my supervisors, Barna Babik and Ferenc Peták for introducing me to clinical research. I greatly appreciate the opportunities they provided to me.
I thank the colleagues at the Department of Anaesthesiology and Intensive Therapy for facilitating my work.
I would like to thank Laura Lászik for her contributions in reviewing the English version.
I am grateful to my family for their continuous encouragement.

REFERENCES

1. Ortega R, Connor C, Kim S, et al. Monitoring ventilation with capnography. N Engl J Med 2012;367(19):e27.
2. Thompson JE, Jaffe MB. Capnographic waveforms in the mechanically ventilated patient. Respir Care 2005;50(1):100-108; discussion 108-109.
3. Pfund AH, Gemill C. An infrared absorption method for the quantitative analysis of respiratory and other gases. Bull Johns Hopkins Hosp 1940;67:61-65.
4. Elam JO, Brown ES, Ten Pas RH. Carbon dioxide homeostasis during anesthesia. I. Instrumentation. Anesthesiology 1955;16(6):876-885.
5. B S. Capnografie (Thesis). In. University of Utrecht: A Oosthoek Publishing Company; 1967.
6. Weingarten M. Respiratory monitoring of carbon dioxide and oxygen: a ten-year perspective. J Clin Monit 1990;6(3):217-225.
7. Kinsella SM. Assessment of the Hewlett-Packard HP47210A capnometer. Br J Anaesth 1985;57(9):919-923.
8. Babik B, Csorba Z, Czovek D, et al. Effects of respiratory mechanics on the capnogram phases: importance of dynamic compliance of the respiratory system. Crit Care 2012;16(5):R177.
9. Kasuya Y, Akca O, Sessler DI, et al. Accuracy of postoperative end-tidal Pco2 measurements with mainstream and sidestream capnography in non-obese patients and in obese patients with and without obstructive sleep apnea. Anesthesiology 2009;111(3):609-615.
10. Brown RH, Brooker A, Wise RA, et al. Forced expiratory capnography and chronic obstructive pulmonary disease (COPD). J Breath Res 2013;7(1):017108.
11. Krauss B, Deykin A, Lam A, et al. Capnogram shape in obstructive lung disease. Anesth Analg 2005;100(3):884-888, table of contents.
12. Kupnik D, Skok P. Capnometry in the prehospital setting: are we using its potential? Emerg Med J 2007;24(9):614-617.
13. Krauss B, Hess DR. Capnography for procedural sedation and analgesia in the emergency department. Ann Emerg Med 2007;50(2):172-181.
14. Eipe N. A review of pediatric capnography. J Clin Monit Comput 2010;4:261268.
15. Balogh AL, Petak F, Fodor GH, et al. Sevoflurane Relieves Lung Function Deterioration After Cardiopulmonary Bypass. J Cardiothorac Vasc Anesth 2017;31(6):2017-2026.
16. Balogh AL, Petak F, Fodor GH, et al. Capnogram slope and ventilation dead space parameters: comparison of mainstream and sidestream techniques. Br J Anaesth 2016;117(1):109-117.
17. Csorba Z, Petak F, Nevery K, et al. Capnographic Parameters in Ventilated Patients: Correspondence with Airway and Lung Tissue Mechanics. Anesth Analg 2016;122(5):1412-1420.
18. Sudy R, Petak F, Kiss L, et al. Obesity and diabetes: similar respiratory mechanical but different gas exchange defects. Am J Physiol Lung Cell Mol Physiol 2021;320(3):L368-L376.

19. Bohm SH, Maisch S, von Sandersleben A, et al. The effects of lung recruitment on the Phase III slope of volumetric capnography in morbidly obese patients. Anesth Analg 2009;109(1):151-159.
20. Tusman G, Groisman I, Fiolo FE, et al. Noninvasive monitoring of lung recruitment maneuvers in morbidly obese patients: the role of pulse oximetry and volumetric capnography. Anesth Analg 2014;118(1):137-144.
21. Tusman G, Gogniat E, Bohm SH, et al. Reference values for volumetric capnography-derived non-invasive parameters in healthy individuals. J Clin Monit Comput 2013;27(3):281-288.
22. Block FE, Jr., McDonald JS. Sidestream versus mainstream carbon dioxide analyzers. J Clin Monit 1992;8(2):139-141.
23. MB J. Mainstream or sidestream capnography. Respironics, Inc 2002;www.oem.respironics.com.
24. Pascucci RC, Schena JA, Thompson JE. Comparison of a sidestream and mainstream capnometer in infants. Crit Care Med 1989;17(6):560-562.
25. Szaflarski NL, Cohen NH. Use of capnography in critically ill adults. Heart Lung 1991;20(4):363-372.
26. Ward KR, Yealy DM. End-tidal carbon dioxide monitoring in emergency medicine, Part 2: Clinical applications. Acad Emerg Med 1998;5(6):637-646.
27. Breen PH, Mazumdar B, Skinner SC. Capnometer transport delay: measurement and clinical implications. Anesth Analg 1994;78(3):584-586.
28. From RP, Scamman FL. Ventilatory frequency influences accuracy of end-tidal CO2 measurements. Analysis of seven capnometers. Anesth Analg 1988;67(9):884-886.
29. Bhavani-Shankar K, Philip JH. Defining segments and phases of a time capnogram. Anesth Analg 2000;91(4):973-977.
30. Anderson CT, Breen PH. Carbon dioxide kinetics and capnography during critical care. Crit Care 2000;4(4):207-215.
31. Walsh BK, Crotwell DN, Restrepo RD. Capnography/Capnometry during mechanical ventilation: 2011. Respir Care 2011;56(4):503-509.
32. Romero PV, Rodriguez B, de Oliveira D, et al. Volumetric capnography and chronic obstructive pulmonary disease staging. Int J Chron Obstruct Pulmon Dis 2007;2(3):381-391.
33. Blanch L, Romero PV, Lucangelo U. Volumetric capnography in the mechanically ventilated patient. Minerva Anestesiol 2006;72(6):577-585.
34. Tusman G, Scandurra A, Bohm SH, et al. Model fitting of volumetric capnograms improves calculations of airway dead space and slope of phase III. J Clin Monit Comput 2009;23(4):197-206.
35. Romero PV, Lucangelo U, Lopez Aguilar J, et al. Physiologically based indices of volumetric capnography in patients receiving mechanical ventilation. Eur Respir J 1997;10(6):1309-1315.
36. Tusman G, Suarez-Sipmann F, Bohm SH, et al. Capnography reflects ventilation/perfusion distribution in a model of acute lung injury. Acta Anaesthesiol Scand 2011;55(5):597-606.

37. Merilainen P, Hanninen H, Tuomaala L. A novel sensor for routine continuous spirometry of intubated patients. J Clin Monit 1993;9(5):374-380.
38. Fletcher R, Jonson B. Deadspace and the single breath test for carbon dioxide during anaesthesia and artificial ventilation. Effects of tidal volume and frequency of respiration. Br J Anaesth 1984;56(2):109-119.
39. Tusman G, Areta M, Climente C, et al. Effect of pulmonary perfusion on the slopes of single-breath test of CO2. J Appl Physiol (1985) 2005;99(2):650-655.
40. Kars AH, Bogaard JM, Stijnen T, et al. Dead space and slope indices from the expiratory carbon dioxide tension-volume curve. Eur Respir J 1997;10(8):1829-1836.
41. Tusman G, Bohm SH, Suarez-Sipmann F, et al. Alveolar recruitment improves ventilatory efficiency of the lungs during anesthesia. Can J Anaesth 2004;51(7):723-727.
42. Stromberg NO, Gustafsson PM. Ventilation inhomogeneity assessed by nitrogen washout and ventilation-perfusion mismatch by capnography in stable and induced airway obstruction. Pediatr Pulmonol 2000;29(2):94-102.
43. Bohr C. Über die Lungenatmung. Skan Arch Physiol 1891;53:236-238.
44. Fletcher R, Jonson B, Cumming G, et al. The concept of deadspace with special reference to the single breath test for carbon dioxide. Br J Anaesth 1981;53(1):77-88.
45. Fowler W. The respiratory dead space. Am J Physiol 1948;54:405-416.
46. Enghoff H. Volumen inefficax. Uppsala Laekareforen Forh 1938;44:191-218.
47. Fowler WS. Lung function studies; the respiratory dead space. Am J Physiol 1948;154(3):405-416.
48. Hedenstierna G, Sandhagen B. Assessing dead space. A meaningful variable? Minerva Anestesiol 2006;72(6):521-528.
49. Tusman G, Sipmann FS, Bohm SH. Rationale of dead space measurement by volumetric capnography. Anesth Analg 2012;114(4):866-874.
50. Lorx A IP. Monitorozás lélegeztetés alatt. In: I. P, A. L, editors. A lélegeztetés elmélete és gyakorlata. Budapest: Medicina Könyvkiadó Rt.; 2004.
51. Shankar KB, Moseley H, Kumar Y, et al. Arterial to end tidal carbon dioxide tension difference during caesarean section anaesthesia. Anaesthesia 1986;41(7):698-702.
52. Russell GB, Graybeal JM, Strout JC. Stability of arterial to end-tidal carbon dioxide gradients during postoperative cardiorespiratory support. Can J Anaesth 1990;37(5):560-566.
53. Bhavani-Shankar K, Moseley H, Kumar AY, et al. Capnometry and anaesthesia. Can J Anaesth 1992;39(6):617-632.
54. Neumar RW, Otto CW, Link MS, et al. Part 8: adult advanced cardiovascular life support: 2010 American Heart Association Guidelines for Cardiopulmonary Resuscitation and Emergency Cardiovascular Care. Circulation 2010;122(18 Suppl 3):S729-767.
55. Poirier MP, Gonzalez Del-Rey JA, McAneney CM, et al. Utility of monitoring capnography, pulse oximetry, and vital signs in the detection of airway mishaps: a hyperoxemic animal model. Am J Emerg Med 1998;16(4):350-352.

56. Hall D, Goldstein A, Tynan E, et al. Profound hypercarbia late in the course of laparoscopic cholecystectomy: detection by continuous capnometry. Anesthesiology 1993;79(1):173-174.
57. Zhou F, Yu T, Du R, et al. Clinical course and risk factors for mortality of adult inpatients with COVID-19 in Wuhan, China: a retrospective cohort study. Lancet 2020;395(10229):1054-1062.
58. Lee CCM, Thampi S, Lewin B, et al. Battling COVID-19: critical care and peri-operative healthcare resource management strategies in a tertiary academic medical centre in Singapore. Anaesthesia 2020.
59. Wang Y, Lu X, Li Y, et al. Clinical Course and Outcomes of 344 Intensive Care Patients with COVID-19. Am J Respir Crit Care Med 2020;201(11):1430-1434.
60. Richardson S, Hirsch JS, Narasimhan M, et al. Presenting Characteristics, Comorbidities, and Outcomes Among 5700 Patients Hospitalized With COVID-19 in the New York City Area. JAMA 2020;323(20):2052-2059.
61. Korsos A, Kupcsulik S, Lovas A, et al. Diagnostic consideration and bedside estimation of the prognosis in COVID-19 patients. Orv Hetil 2020;161(17):667-671.
62. Wendel Garcia PD, Aguirre-Bermeo H, Buehler PK, et al. Implications of early respiratory support strategies on disease progression in critical COVID-19: a matched subanalysis of the prospective RISC-19-ICU cohort. Crit Care 2021;25(1):175.
63. Sanche S, Lin YT, Xu C, et al. High Contagiousness and Rapid Spread of Severe Acute Respiratory Syndrome Coronavirus 2. Emerg Infect Dis 2020;26(7).
64. Park M, Cook AR, Lim JT, et al. A Systematic Review of COVID-19 Epidemiology Based on Current Evidence. J Clin Med 2020;9(4).
65. Brochard L, Slutsky A, Pesenti A. Mechanical Ventilation to Minimize Progression of Lung Injury in Acute Respiratory Failure. Am J Respir Crit Care Med 2017;195(4):438-442.
66. Gattinoni L, Coppola S, Cressoni M, et al. Covid-19 Does Not Lead to a "Typical" Acute Respiratory Distress Syndrome. Am J Respir Crit Care Med 2020.
67. Marini JJ, Gattinoni L. Management of COVID-19 Respiratory Distress. JAMA 2020.
68. Wax RS, Christian MD. Practical recommendations for critical care and anesthesiology teams caring for novel coronavirus (2019-nCoV) patients. Can J Anaesth 2020;67(5):568-576.
69. Wilcox SR. Management of respiratory failure due to covid-19. BMJ 2020;369:m1786.
70. Bhatraju PK, Ghassemieh BJ, Nichols M, et al. Covid-19 in Critically Ill Patients in the Seattle Region - Case Series. N Engl J Med 2020.
71. Chen N, Zhou M, Dong X, et al. Epidemiological and clinical characteristics of 99 cases of 2019 novel coronavirus pneumonia in Wuhan, China: a descriptive study. Lancet 2020;395(10223):507-513.
72. Neyman G, Irvin CB. A single ventilator for multiple simulated patients to meet disaster surge. Acad Emerg Med 2006;13(11):1246-1249.
73. Paladino L, Silverberg M, Charchaflieh JG, et al. Increasing ventilator surge capacity in disasters: ventilation of four adult-human-sized sheep on a single ventilator with a modified circuit. Resuscitation 2008;77(1):121-126.

74. Clarke AL, Stephens AF, Liao S, et al. Coping with COVID-19: ventilator splitting with differential driving pressures using standard hospital equipment. Anaesthesia 2020.
75. Chatburn RL, Branson RD, Hatipoglu U. Multiplex Ventilation: A Simulation-based Study of Ventilating Two Patients with One Ventilator. Respir Care 2020.
76. Collaboration NCDRF. Worldwide trends in diabetes since 1980: a pooled analysis of 751 population-based studies with 4.4 million participants. Lancet 2016;387(10027):1513-1530.
77. Ogurtsova K, da Rocha Fernandes JD, Huang Y, et al. IDF Diabetes Atlas: Global estimates for the prevalence of diabetes for 2015 and 2040. Diabetes Res Clin Pract 2017;128:40-50.
78. Sjoding MW, Prescott HC, Wunsch H, et al. Longitudinal Changes in ICU Admissions Among Elderly Patients in the United States. Crit Care Med 2016;44(7):1353-1360.
79. Abd-Elrahman KS, Walsh MP, Cole WC. Abnormal Rho-associated kinase activity contributes to the dysfunctional myogenic response of cerebral arteries in type 2 diabetes. Can J Physiol Pharmacol 2015;93(3):177-184.
80. Rask-Madsen C, King GL. Vascular complications of diabetes: mechanisms of injury and protective factors. Cell Metab 2013;17(1):20-33.
81. Xu RS. Pathogenesis of diabetic cerebral vascular disease complication. World J Diabetes 2015;6(1):54-66.
82. Gregg EW, Li Y, Wang J, et al. Changes in diabetes-related complications in the United States, 1990-2010. N Engl J Med 2014;370(16):1514-1523.
83. Giacco F, Brownlee M. Oxidative stress and diabetic complications. Circ Res 2010;107(9):1058-1070.
84. Brownlee M. The pathobiology of diabetic complications: a unifying mechanism. Diabetes 2005;54(6):1615-1625.
85. Paneni F, Beckman JA, Creager MA, et al. Diabetes and vascular disease: pathophysiology, clinical consequences, and medical therapy: part I. Eur Heart J 2013;34(31):2436-2443.
86. Brownlee M. Biochemistry and molecular cell biology of diabetic complications. Nature 2001;414(6865):813-820.
87. Stirban A, Gawlowski T, Roden M. Vascular effects of advanced glycation endproducts: Clinical effects and molecular mechanisms. Mol Metab 2014;3(2):94-108.
88. El-Yazbi AF, Abd-Elrahman KS. ROK and Arteriolar Myogenic Tone Generation: Molecular Evidence in Health and Disease. Front Pharmacol 2017;8:87.
89. Lecube A, Simo R, Pallayova M, et al. Pulmonary Function and Sleep Breathing: Two New Targets for Type 2 Diabetes Care. Endocr Rev 2017;38(6):550-573.
90. Devaskar SU, DeMello DE. Cell-specific localization of glucose transporter proteins in mammalian lung. Journal of Clinical Endocrinology & Metabolism 1996;81(12):4373-4378.
91. Martin-Frias M, Lamas A, Lara E, et al. Pulmonary function in children with type 1 diabetes mellitus. J Pediatr Endocrinol Metab 2015;28(1-2):163-169.
92. Schnapf BM, Banks RA, Silverstein JH, et al. Pulmonary function in insulin-dependent diabetes mellitus with limited joint mobility. Am Rev Respir Dis 1984;130(5):930-932.

93. Wanke T, Formanek D, Auinger M, et al. Inspiratory muscle performance and pulmonary function changes in insulin-dependent diabetes mellitus. Am Rev Respir Dis 1991;143(1):97-100.
94. Kuziemski K, Slominski W, Jassem E. Impact of diabetes mellitus on functional exercise capacity and pulmonary functions in patients with diabetes and healthy persons. BMC Endocr Disord 2019;19(1):2.
95. van Gent R, Brackel HJ, de Vroede M, et al. Lung function abnormalities in children with type I diabetes. Respir Med 2002;96(12):976-978.
96. Antonelli Incalzi R, Fuso L, Giordano A, et al. Neuroadrenergic denervation of the lung in type I diabetes mellitus complicated by autonomic neuropathy. Chest 2002;121(2):443-451.
97. Bertherat J, Lubetzki J, Lockhart A, et al. Decreased bronchial response to methacholine in IDDM patients with autonomic neuropathy. Diabetes 1991;40(9):1100-1106.
98. Mancini M, Filippelli M, Seghieri G, et al. Respiratory muscle function and hypoxic ventilatory control in patients with type I diabetes. Chest 1999;115(6):1553-1562.
99. Eaton T, Withy S, Garrett JE, et al. Spirometry in primary care practice: the importance of quality assurance and the impact of spirometry workshops. Chest 1999;116(2):416-423.
100. Giner J, Plaza V, Rigau J, et al. Spirometric standards and patient characteristics: an exploratory study of factors affecting fulfillment in routine clinical practice. Respir Care 2014;59(12):1832-1837.
101. Babik B, Petak F, Asztalos T, et al. Components of respiratory resistance monitored in mechanically ventilated patients. Eur Respir J 2002;20(6):1538-1544.
102. Phua J, Weng L, Ling L, et al. Intensive care management of coronavirus disease 2019 (COVID-19): challenges and recommendations. Lancet Respir Med 2020.
103. Xie J, Tong Z, Guan X, et al. Critical care crisis and some recommendations during the COVID-19 epidemic in China. Intensive Care Med 2020.
104. Carenzo L, Costantini E, Greco M, et al. Hospital surge capacity in a tertiary emergency referral centre during the COVID-19 outbreak in Italy. Anaesthesia 2020.
105. Abid A, Mieloszyk RJ, Verghese GC, et al. Model-Based Estimation of Respiratory Parameters from Capnography, With Application to Diagnosing Obstructive Lung Disease. IEEE Trans Biomed Eng 2017;64(12):2957-2967.
106. Oliveira TL, Candeia-Medeiros N, Cavalcante-Araujo PM, et al. SGLT1 activity in lung alveolar cells of diabetic rats modulates airway surface liquid glucose concentration and bacterial proliferation. Sci Rep 2016;6:21752.
107. Duncan BB, Schmidt MI, Pankow JS, et al. Low-grade systemic inflammation and the development of type 2 diabetes: the atherosclerosis risk in communities study. Diabetes 2003;52(7):1799-1805.
108. Schmidt MI, Duncan BB, Sharrett AR, et al. Markers of inflammation and prediction of diabetes mellitus in adults (Atherosclerosis Risk in Communities study): a cohort study. Lancet 1999;353(9165):1649-1652.
109. Singh S, Bodas M, Bhatraju NK, et al. Hyperinsulinemia adversely affects lung structure and function. Am J Physiol Lung Cell Mol Physiol 2016;310(9):L837-845.

110. Wang CC, Gurevich I, Draznin B. Insulin affects vascular smooth muscle cell phenotype and migration via distinct signaling pathways. Diabetes 2003;52(10):2562-2569.
111. Douglas NJ, Campbell IW, Ewing DJ, et al. Reduced airway vagal tone in diabetic patients with autonomic neuropathy. Clin Sci (Lond) 1981;61(5):581-584.
112. Sudy R, Schranc A, Fodor GH, et al. Lung volume dependence of respiratory function in rodent models of diabetes mellitus. Respir Res 2020;21(1):82.
113. Babik B, Petak F, Agocs S, et al. [Diabetes mellitus: endothelial dysfunction and changes in hemostasis]. Orv Hetil 2018;159(33):1335-1345.
114. Peters U, Dechman G, Hernandez P, et al. Improvement in upright and supine lung mechanics with bariatric surgery affects bronchodilator responsiveness and sleep quality. J Appl Physiol (1985) 2018.
115. Kalchiem-Dekel O, Hines SE. Forty years of reference values for respiratory system impedance in adults: 1977-2017. Respir Med 2018;136:37-47.
116. Rivas E, Arismendi E, Agusti A, et al. Ventilation/Perfusion distribution abnormalities in morbidly obese subjects before and after bariatric surgery. Chest 2015;147(4):1127-1134.
117. Boriek AM, Lopez MA, Velasco C, et al. Obesity modulates diaphragm curvature in subjects with and without COPD. Am J Physiol Regul Integr Comp Physiol 2017;313(5):R620-R629.